A mio marito.

Contents

Introduction

During the three years of Ph.D. I have been involved in the modellization of the light behavior in a Liquid Crystal (LC) cell and relative molecular director configuration in particular, complex, geometries. The studied configurations (boundary condition of light beams and director orientation inside the cells) are related to actual experimental problems treated in our laboratory.

In order to provide a clear presentation of my work I have divided it in three different chapter:

- The first one is related to reorientational effects in a NLC cell undergoing **multiple irradiation**
- The second one is related to simulation of light propagation in **periodic and non-periodic potentials**
- The thirth one concerns the derivation of director configuration in a NLC cell with **multiple interfaces**

In all cases, I have studied the interaction between the optical field and the Nematic Liquid Crystal.

I Basis of non-linear optical properties of LC

For a microscopic point of view, the Nematic Liquid Crystals (NLCs) are liquid materials with rod-like (or disk-like) molecules and an angular correlation function that assumes a value different from zero for a distance $\xi \sim d$ ($d =$ distance of first neighbor molecules). This means that the Liquid Crystals show a reorientational order and some times a positional order that can be described through an **order parameter**, which assumes zero value for an isotropic phase and non-zero values for the liquid crystal phase. Liquid Crystal molecules provide a cooperative response to an external stress and therefore it is useful to define the **molecular director** $\mathbf{n}$. This vector represents the average molecular direction in a volume that is small enough if compared to the sample volume (several cm) and big enough if compared to the molecular length (~ 20 Å). From a macroscopic point of view, a tipical difference between a high-temperature isotropic liquid and the nematic phase is found in the determination of all macroscopic tensor properties. A response function like the dielectric or the magnetic permittivity results to be the best candidate to define the order parameter. The electric response of the material to an external field is described by the tensor

$$\varepsilon_{ij} = \varepsilon_{\perp}\delta_{ij} + (\varepsilon_{\parallel} - \varepsilon_{\perp})n_i n_j \tag{1}$$

where n_i are the components of the molecular director and $\varepsilon_{\perp}, \varepsilon_{\parallel}$ represent the dielectric response to an electric field respectively perpendicular and parallel to the molecular director.

In many circumstances, the induced energy variation per molecule is small in comparison to the intermolecular potential and significant variations of $\mathbf{n}$ occur over distances much larger than the molecular scale. In this framework, we can use the

Continuum theory and treat the molecular director $\mathbf{n}$ as a continuum function of coordinates in order to derive the macroscopic physical properties as a function of local molecular director orientation. The continuum theory can describe the liquid crystal deformation without taking into account the details of the structure and interactions on a molecular scale. In the framework of this macroscopic approach the equilibrium states of a liquid crystal are found by minimization of an appropriate thermodynamic potential, the *free energy*, $\mathcal{F}$ defined as [2]

$$\mathcal{F} = U - TS \tag{2}$$

where U is the internal energy, and S the entropy of the system at the absolute temperature T. In the continuum theory, the usual form of the bulk *elastic free energy density* of a nematic liquid crystal was given by Frank [1]

$$\mathcal{F}_K = \frac{K_1}{2}(\nabla \cdot \mathbf{n})^2 + \frac{K_2}{2}(\mathbf{n} \cdot \nabla \times \mathbf{n})^2 + \frac{K_3}{2}(\mathbf{n} \times \nabla \times \mathbf{n})^2 \tag{3}$$

where K_1, K_2, K_3 are respectively the splay, twist and bend elastic constants, which are always positive, have dimension of energy/length (*i.e.*, of a force) and their magnitude has been found to be of the order of $10^{-12}N$. When external fields are introduced, besides $\mathcal{F}_K$, it is necessary to take into account also the appropriate free energy density $\mathcal{F}_E$ due to the interaction between liquid crystal molecules and the applied field. In this case, the free energy density becomes the sum of two terms: the first due to the elastic deformation and the second, due to the field induced deformation

$$\mathcal{F}\left(\mathbf{n}, \nabla\mathbf{n}\right) = \mathcal{F}_K + \mathcal{F}_E \tag{4}$$

The energy density due to the interaction with an electrical static field is written as

$$\mathcal{F}_E = -\int \mathbf{D} \cdot d\mathbf{E} = -\frac{\varepsilon_0}{2}\int \varepsilon_{ik} E_i \, dE_k = -\varepsilon_0\varepsilon_\perp \frac{E^2}{2} - \frac{\varepsilon_0 \Delta\varepsilon}{2}\left(\mathbf{n} \cdot \mathbf{E}\right)^2 \tag{5}$$

An electromagnetic (e.m.) wave brings both electric and magnetic field but the liquid crystal interacts only with the electric field and, in any case, the orientig action of the magnetic field is negligible if compared to the one of the electric field and can be neglected. For a high frequency field $\mathbf{E} = (1/2)\left[\mathbf{E}_0 e^{-i\omega t} + c.c.\right]$ the product $E_i E_k$ becomes $(1/2)\, E_1 E_k^{\star}$ and the free energy density due to the LC interaction with the optical field becomes

$$\mathcal{F}_{e.m.} = -\frac{\varepsilon_0 \varepsilon_{\perp}}{4} |\mathbf{E}|^2 - \frac{\varepsilon_0 \Delta\varepsilon}{4} (\mathbf{n}\cdot\mathbf{E})(\mathbf{n}\cdot\mathbf{E}^{\star}) \tag{6}$$

The total energy density due to each contribute is therefore

$$\begin{aligned}
\mathcal{F}(\mathbf{n}, \nabla\mathbf{n}) &= \mathcal{F}_K + \mathcal{F}_{e.m.} + \mathcal{F}_E = \\
&= \frac{K_1}{2}(\nabla\cdot\mathbf{n})^2 + \frac{K_2}{2}(\mathbf{n}\cdot\nabla\times\mathbf{n})^2 + \frac{K_3}{2}(\mathbf{n}\times\nabla\times\mathbf{n})^2 + \\
&\quad - \frac{\varepsilon_0 \varepsilon_{\perp}^{hf}}{4} |\mathbf{E}|^2 - \frac{\varepsilon_0 \Delta\varepsilon^{hf}}{4} (\mathbf{n}\cdot\mathbf{E})(\mathbf{n}\cdot\mathbf{E}^{\star}) + \\
&\quad - \varepsilon_0 \varepsilon_{\perp}^{lf} \frac{E^2}{2} - \frac{\varepsilon_0 \Delta\varepsilon^{lf}}{2} (\mathbf{n}\cdot\mathbf{E})^2
\end{aligned} \tag{7}$$

When the system is dynamically isolated (zero value of the mechanical work L i.e. $L = 0$) and remains at a constant temperature, then, the free energy cannot increase:

$$\Delta\mathcal{F} \leq 0, \tag{8}$$

If the free energy is in a minimum, the system is in a state of equilibrium; then, the equilibrium configuration of $\mathbf{n}(\mathbf{r})$ is found by applying the methods of variational calculus, namely, by minimizing $\mathcal{F}$. This procedure leads to the *Eulero-Lagrange equations*. Expressing $\mathbf{n}$ as a function of Euler angles (θ, ϕ), which determine the vector orientation, then the Eulero-Lagrange equation becomes:

$$\frac{\partial\mathcal{F}}{\partial q^i} - \sum_{\beta} \frac{\partial}{\partial x_\beta} \frac{\partial\mathcal{F}}{\partial\left(\partial q^i / \partial x_\beta\right)} = 0 \tag{9}$$

where q^i are the considered Euler angles and, from a more general point of view, represent the choosen thermodynamical coordinates, while x_β are the spatial variables. The former Equation is valid for the equilibrium configuration in steady state condition. When the transient behavior has to be studied, a dissipative term must be included on the right:

$$\frac{\partial \mathcal{F}}{\partial q^i} - \sum_\beta \frac{\partial}{\partial x_\beta} \frac{\partial \mathcal{F}}{\partial \left(\partial q^i / \partial x_\beta\right)} = -R_{ij} \frac{\partial q^i}{\partial t} \tag{10}$$

where t is the temporal variable and R_{ij} has been introduced to take into account the energy dissipation.

Equations (9), (10) must be integrated with conditions for the director orientation at the walls which limit the sample. These conditions are given by the type of interaction existing between the liquid crystal molecules and the substrate. The strength of the interfacial interaction is a fundamental feature which must be taken account, because it affects the result of the application of external fields to the director and, as a consequence, it determines the macroscopic response of the medium. Often, the approximation of *strong anchoring* is made, which means that the director orientationat at the boundary is supposedly fixed and indipendent of the external exitation. In this case, the boundary conditions are simply given by the values of n_x, n_y, n_z (or of the correspondent Euler angles θ and ϕ) at the limiting substrates, and Equations (9), (10) must be solved under these constraints. There are situations (in particular, if the thickness of the sample is small) where this approximation fails. It means that it is not possible to consider an infinite anchoring energy like in the previous case, but a surface condition contribution must be included in the free energy. In general this is done [3, 4] by adding a free energy density for unit surface

area, written as

$$\mathcal{G} = \int_{d/2}^{-d/2} \mathcal{F}\left(\theta, \phi, \theta_z, \phi_z\right)\, dz \; + \mathcal{F}_1^s + \mathcal{F}_2^s \tag{11}$$

In equation (11), the z-axis is normal to the boundary surfaces and the plane $z = 0$ is chosen at the centre of the cell of thickness d, we have indicated $\theta_z = d\theta/dz$ and $\phi_z = d\phi/dz$. The surface terms $\mathcal{F}_1^s$ and $\mathcal{F}_2^s$ are functions of θ and ϕ. Minimizing $\mathcal{G}$ we obtain the steady state condition for the Euler angles to the surface $d/2$ and $-d/2$. Therefore the Euler-Lagrange equations (9), (10) must be solved with the following boundary conditions

$$\frac{\partial \mathcal{F}}{\partial \theta_z} - \frac{\partial \mathcal{F}_1^s}{\partial \theta} = 0 \tag{12}$$

$$\frac{\partial \mathcal{F}}{\partial \phi_z} - \frac{\partial \mathcal{F}_1^s}{\partial \phi} = 0 \tag{13}$$

at $z = -d/2$, and

$$\frac{\partial \mathcal{F}}{\partial \theta_z} + \frac{\partial \mathcal{F}_2^s}{\partial \theta} = 0 \tag{14}$$

$$\frac{\partial \mathcal{F}}{\partial \phi_z} + \frac{\partial \mathcal{F}_2^s}{\partial \phi} = 0 \tag{15}$$

at $z = d/2$. Of course, in order to solve equations (9) together with the boundary conditions (13) and (15) it is necessary to know the explicit form of $\mathcal{F}_1^s$ and $\mathcal{F}_2^s$. Actually, the correct choice of these functions, with the obvious constraint that they must have a minimum for the "easy angles" θ_0 and ϕ_0 at the surface is a very important problem. In many cases [4], $\mathcal{F}^s$ is chosen as a series expansion in the form

$$\begin{aligned} \mathcal{F}^s(\theta) =& (1/2)W_{s1}\sin^2(\theta - \theta_0) + (1/2)W_{s2}\sin^4(\theta - \theta_0) \\ &+ (1/2)W_{s3}\sin^6(\theta - \theta_0) + \ldots \end{aligned} \tag{16}$$

and a similar for ϕ:

$$\begin{aligned}\mathcal{F}^s(\phi) =&(1/2)W_{s1}\sin^2(\phi-\phi_0)+(1/2)W_{s2}\sin^4(\phi-\phi_0)\\&+(1/2)W_{s3}\sin^6(\phi-\phi_0)+\ldots\end{aligned} \tag{17}$$

Under the Rapini [5] approximation of a small deviation from the easy angle at the surface, equation (16)reduces to

$$\begin{aligned}\mathcal{F}^s(\theta) &= (1/2)W_{s1}\sin^2(\theta-\theta_0)\\ \mathcal{F}^s(\phi) &= (1/2)W_{s1}\sin^2(\phi-\phi_0)\end{aligned} \tag{18}$$

where W_{s1} is called polar anchoring energy, while the correspondent equation for ϕ defines the azimuthal anchoring energy. The energy anchoring has a wide range of possible values in liquid crystal interfaces going from 1 to $10^2 J/m^2$; depending on the neture of the interaction with substrate.

II Basic non-linear optics

The evolution of electric and magnetic fields is described by the Maxwell's equations that in a uniform anisotropic medium become:

$$\nabla\cdot\mathbf{D}=\rho \tag{19}$$

$$\nabla\times\mathbf{E}=-\frac{\partial\mathbf{B}}{\partial t} \tag{20}$$

$$\nabla\cdot\mathbf{B}=0 \tag{21}$$

$$\nabla\times\mathbf{H}=\mathbf{J}+\frac{\partial\mathbf{D}}{\partial t} \tag{22}$$

where ρ is the free charge density, J is the electric current density, $\mathbf{D}$ and $\mathbf{B}$ are the electric and magnetic displacement vectors, $\mathbf{E}$ and $\mathbf{H}$ are the electric and magnetic

field vectors. The material response to an electromagnetic field is summarized in the constitutive relations:

$$\mathbf{D} = \underline{\varepsilon}\mathbf{E} \tag{23}$$

$$\mathbf{B} = \underline{\mu}\mathbf{H} \tag{24}$$

$$\mathbf{J} = \underline{\sigma}\mathbf{E} \tag{25}$$

where σ is the conductibility, $\underline{\varepsilon}$, $\underline{\mu}$ are tensors that describe the electric and magnetic response of the material to fields; the tensorial character allows us to describe also anisotropic materials like Liquid Crystals. If $\varepsilon(\mathbf{r}, t)$ is know, then the Spatial Maxwell wave equation allows us to describe the evolution of the electric field:

$$\nabla^2\mathbf{E} + \frac{\omega^2}{c^2}\underline{\varepsilon}_r\mathbf{E} = 0 \tag{26}$$

There are several situations where an analytical approach can be used to get a solution of the Spatial Maxwell wave equation (26). For example, Zel'dovich and coworkers [6] reported the solution for a wave traveling in a inhomogeneous an-isotropic medium under the Geometrical Optical Approximation (GOA) for a linearly polarized wave. In general, however, in the presence of a non linear behavior, the complete solution of equation (26) needs a numerical approach. Different numerical techniques have been implemented for different problems: The propagation in periodic potential is approached with the Floquet-Bloch technique [9–11] born in the framework of solid state physics and used also for other kind of periodic structures (like liquid crystals or polymeric structures).

The finite-difference beam-propagation method (FD-BPM) and the finite - difference time-domain method (FD-TDM) are powerful numerical techniques for analyzing optical waveguide devices. In this framework, since the FD-BPM takes into

account only traveling waves, reflected waves generated at longitudinal discontinuities are neglected. For cases where the reflection cannot be neglected, the bidirectional BPM has been proposed [7, 8]. On the other hand, the FD-TDM introduces no approximation with respect to propagating beam directions, although it requires great computation time and RAM memorie for the simulation of large structures. From this viewpoint, a hybrid simulation started to attract attention. From a general point of view, a good numerical approach has to fulfill the requirement of a good accordance with experimental results and low computation time and Ram memorie needed for the simulation of the structures under analisys. For this reason, the best code for a particular system is the one that can be built around the system, taking into account only the real boundary conditions and the approximation that the system allows to consider. In this three years, my work has been aimed to realize a theoretical support to experimental problem of our Laboratory.

III General Equations

For the three arguments I have investigated, I have I used the same reference system reported in Figure 1. In this system, the molecular director is written (like in (27)) as

$$\hat{\mathbf{n}} = (\sin\theta, \cos\theta\cos\phi, \cos\theta\sin\phi) \tag{27}$$

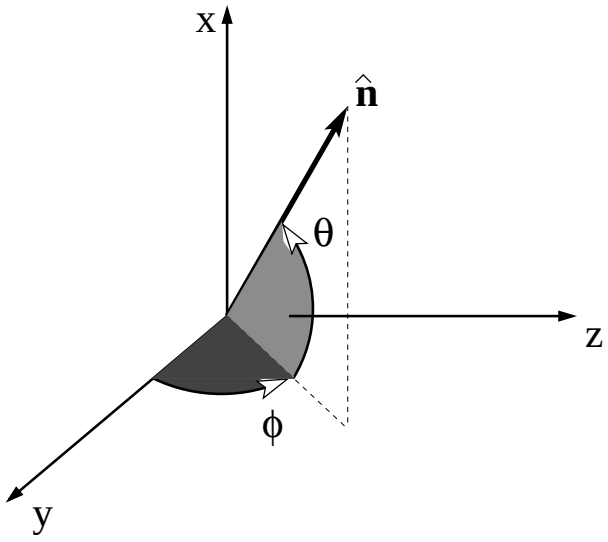

Figure 1: *Reference system used in order to study all the following analyzed systems*

while the dielectric permittivity tensor of eq (1), written as

$$\underline{\varepsilon} = \begin{pmatrix} \varepsilon_{xx} & \varepsilon_{xy} & \varepsilon_{xz} \\ \varepsilon_{yx} & \varepsilon_{yy} & \varepsilon_{yz} \\ \varepsilon_{zx} & \varepsilon_{zy} & \varepsilon_{zz} \end{pmatrix}, \tag{28}$$

becomes

$$\underline{\varepsilon} = \begin{pmatrix} \varepsilon_{\perp} + \Delta\varepsilon \sin^2\theta & \Delta\varepsilon \sin\theta\cos\theta\cos\phi & \Delta\varepsilon \sin\theta\cos\theta\sin\phi \\ \Delta\varepsilon \sin\theta\cos\theta\cos\phi & \varepsilon_{\perp} + \Delta\varepsilon \cos^2\theta\cos^2\phi & \Delta\varepsilon \cos^2\theta\sin\phi\cos\phi \\ \Delta\varepsilon \sin\theta\cos\theta\sin\phi & \Delta\varepsilon \cos^2\theta\sin\phi\cos\phi & \Delta\varepsilon \cos^2\theta\sin^2\phi \end{pmatrix} \tag{29}$$

where $\Delta\varepsilon = \varepsilon_{\parallel} - \varepsilon_{\perp}$.

Applying the Euler-Lagrange equations (10) to total energy density (7) we obtain the Frank's equations for the two angles θ, ϕ that in the most general and compact

case assume the following form (30) and (31)

$$\gamma\frac{\partial\theta}{\partial\tau} = K\nabla^2\theta + K\sin\theta\cos\theta\ \nabla\phi\cdot\nabla\phi - \frac{\varepsilon_0\Delta\varepsilon}{4}\left[\left(\frac{\partial\hat{\mathbf{n}}}{\partial\theta}\cdot\mathbf{E}\right)(\hat{\mathbf{n}}\cdot\mathbf{E}^\star) - (\hat{\mathbf{n}}\cdot\mathbf{E})\left(\frac{\partial\hat{\mathbf{n}}}{\partial\theta}\cdot\mathbf{E}^\star\right)\right] \tag{30}$$

$$\gamma\frac{\partial\phi}{\partial\tau} = K\cos^2\theta\nabla^2\phi - K\sin 2\theta\ \nabla\theta\cdot\nabla\phi - \frac{\varepsilon_0\Delta\varepsilon}{4}\left[\left(\frac{\partial\hat{\mathbf{n}}}{\partial\phi}\cdot\mathbf{E}\right)(\hat{\mathbf{n}}\cdot\mathbf{E}^\star) + (\hat{\mathbf{n}}\cdot\mathbf{E}^\star)\left(\frac{\partial\hat{\mathbf{n}}}{\partial\phi}\cdot\mathbf{E}^\star\right)\right] \tag{31}$$

For normal incidence of the electric field $\mathbf{E} = \mathbf{E}(\mathbf{r})e^{-ikz}$, the Maxwell Equation (26) with the SVEA approximation that means slow varing envelope approximation $|\partial^2\mathbf{E}/\partial z^2| \ll |k\partial\mathbf{E}/\partial z|$ becomes (32)

$$\nabla_\perp^2\mathbf{E}(\mathbf{r}) - 2ik_{iniz}\frac{\partial\mathbf{E}(\mathbf{r})}{\partial z} + \frac{\omega^2}{c^2}(\hat{\varepsilon} - \hat{\varepsilon}_r^{iniz})\mathbf{E}(\mathbf{r}) = 0 \tag{32}$$

where $k_{iniz} = kn_{iniz}$ or $k_{iniz}^2 = k^2\varepsilon_{iniz}$.

For a generic α-algle of incicence the field $\mathbf{E} = \mathbf{E}(\mathbf{r})e^{-i(k_x x + k_z z)}$, the Maxwell Equation (26) with the SVEA approximation $|\partial^2\mathbf{E}/\partial z^2| \ll |k\partial\mathbf{E}/\partial z|$ becomes (33)

$$\frac{\partial^2\mathbf{E}(\mathbf{r})}{\partial x^2} - 2ik_x\frac{\partial\mathbf{E}(\mathbf{r})}{\partial x} - 2ik_z\frac{\partial\mathbf{E}(\mathbf{r})}{\partial z} + \frac{\omega^2}{c^2}(\hat{\varepsilon} - \hat{\varepsilon}_r^{iniz})\mathbf{E}(\mathbf{r}) = 0 \tag{33}$$

IV Modellization of optical radiation-liquid crystal interaction in complex geometries

In the following section are reported a short introduction to the three argument reported in the chapter below.

The first problem has been numerically described with a serial code and regard the problem of multiple irradiation. The second and the third one born to approach the same experimental problem: the optical studies of light propagation in a NLC cell planar aligned with multiple interface and lead to study of light propagation in periodic and non-periodic potentials and derivation of director configuration in a cell with multiple interfaces. In this kind of cell we can observe the formation of spatial solitons, i.e. a self-confined beam whose transverse intensity profile remains unchanged during the propagation. This complex studie requires the realizzation of a big code which optimizzation need the parallelization. In order to learn the parallel thecniques that have allowed me to parallelize my codes during this three year I spent two month in HLRS (High Performance Computing Center) in Stuttgart (Germany) and in the IWM Fraunhofer institute for Mechanics of Materials Freiburg (Germany).

IV.1 Multiple irradiation

The first argument I treated during my doctorate is reported in the first chapter and has produced the publication of two articles .

It treats the reorientational effect in a Nematic Liquid Crystal cell homeotropically aligned which undergoes multiple light interaction. The work has been stimulated by the necessity of studying and characterizing some phenomena observed

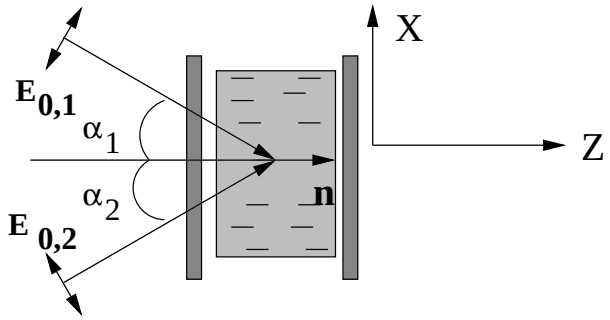

Figure 2: *Nematic Liquid Crystal cell Homeotropic aligned with two beams irradiation*

in our laboratory when two linearly polarized laser beams with a gaussian intensity profile, (plane see Figure. 2) act on a homeotropically aligned NLC cell. We have called these phenomena

- CAW, or Competingly Acting Waves,
- LIFT II, or Light Induced Fréedericksz Transition II,
- Light Charges.

The whole system is described by Maxwell's wave equations for light propagation and by Frank equation for the elastic deformation of the molecular director. The study started from the observations shown in the Figure. 3: Figure. 3(a) corresponds to the well know effect of Self Phase Modulation (SPM) due to birefringence and to the director reorientation induced by the beam. In fact, the laser beam induces a torque on the molecular director and produces a reorientation towards the light polarization direction. The reorientation has the same gaussian profile of the light intensity and yields gaussian refractive index profile (due to birefringence) that produces, at far field, the tipical rings of Self Phase Modulation. Figure. 3(b) and (c) (CAW and LIFT II) are due to the action of two beams impinging on the sample

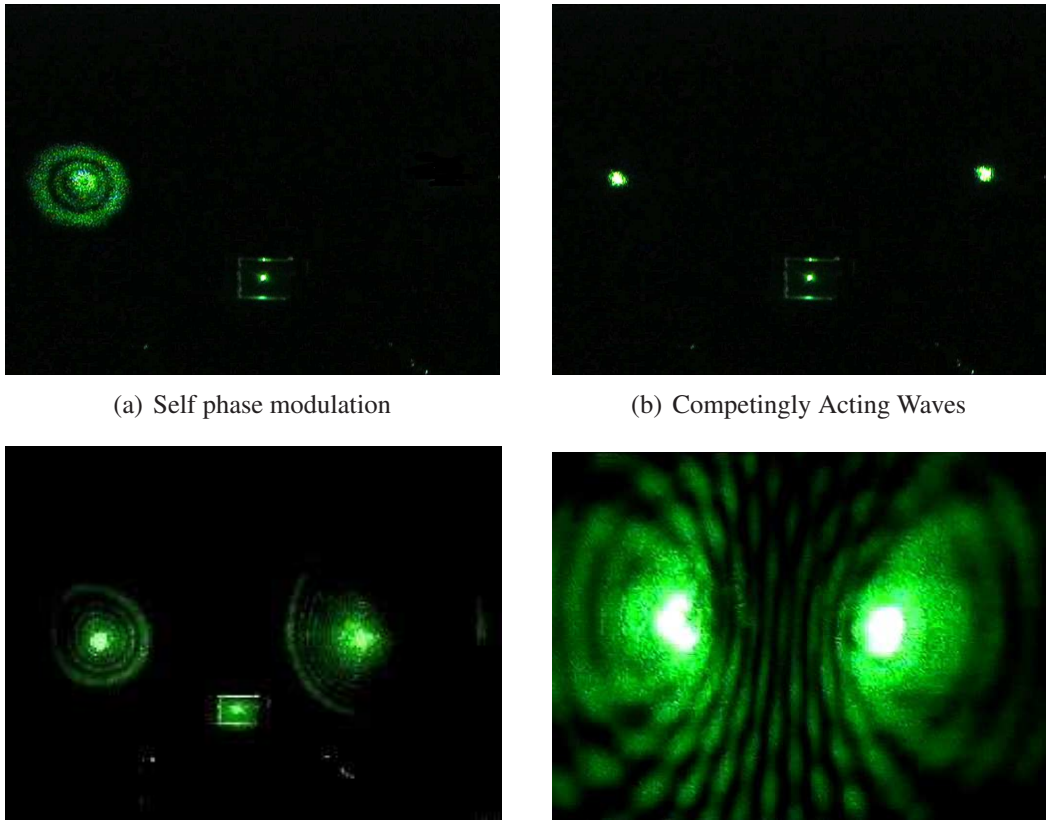

(a) Self phase modulation

(b) Competingly Acting Waves

(c) Light Induced Fréedericksz Transition II

(d) Light Charges

Figure 3: *(a) the far field effect due to action of a laser gaussian beam on a NLC cell homeotropic aligned (b), (c), (d) the far field effect due to action of two beams (b) low light intensity and great angles between the beams (c) high light intensity and great angles between the beams (d) small angles between the beams.*

with great angles (α_1, α_2) (see the Figure. 2). The torque action of the two beams produces two different light behavoirs:

- at low intensity, are in competition and the torque action due to the first one is balanced by the opposit action due to second beam, thus producing a cancellation of the rings;
- at high intensity, torque action due to the second beam amplifies the action due to first one, thus producing an increasing of the rings number.

Figure. 3(d) (Light Charges) corresponds to the action of two beams with small impinging angles (α_1, α_2). In this case, the interfence of the light plays an important role on the effect. The on axis intensity shows an interesting behavior during the ring formation (SPM) and the ring cancellation (CAW) (see Figure 4).

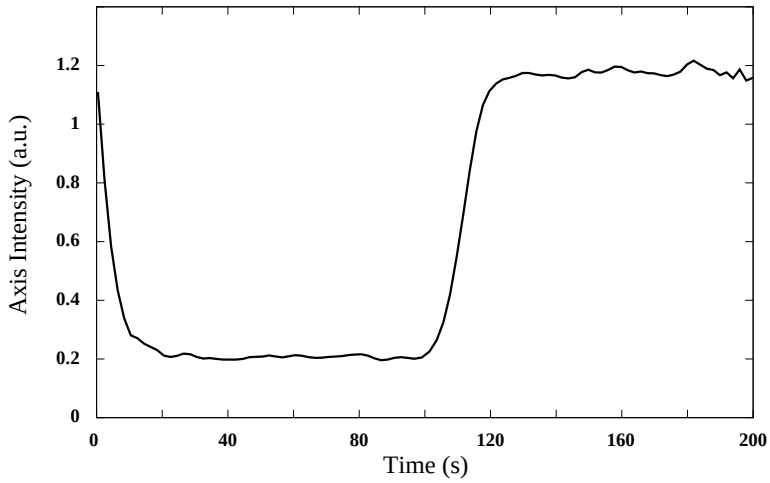

Figure 4: *The axis intensity in arbitrary units versus time during the transient of the ring formation and ring cancellation: during the formation the figure shows a decreasing on axis light intensity; during the cancellation the figure shows an increasing of the light intensity.*

In order to study this kind of phenomena, we observe that the light is linealy polarized in the $x - z$ plane and the NLC is homeotropically aligned; this induces a planar reorientation that can be described with only one θ angle. In general, the electric field $\mathbf{E} = \mathbf{E}(x, z)e^{-i(k_x x + k_z z)}$ propagates along the η-direction $\mathbf{k} = k(\sin\alpha, \cos\alpha) = (k_x, k_z)$ (see Figure 5)

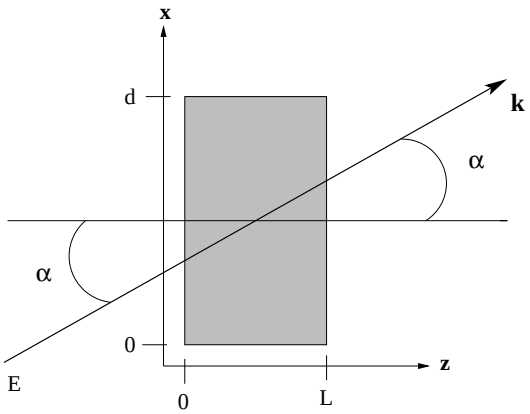

Figure 5: *a rappresentation of the cell and the beam propagation direction*

If only 2 beams act on the sample the equation system which describes the physical system is

$$\begin{aligned}
\gamma\frac{\partial\theta}{\partial t} &= K\nabla^2\theta \quad + \quad \frac{\Delta\varepsilon\varepsilon_0}{4}\left[\sum_{i,j=1}^{N} E_i E_j^* \sin(2\theta-\alpha_i-\alpha_j)\right] \\
\frac{\partial E_1}{\partial z} &= -\frac{i}{2k\cos\alpha}\left[\frac{\partial^2 E_1}{\partial x^2} - 2ik\sin\alpha\frac{\partial E_1}{\partial x} + k^2(n^2(\theta)-1)E_1\right] \qquad (34) \\
\frac{\partial E_2}{\partial z} &= -\frac{i}{2k\cos\alpha}\left[\frac{\partial^2 E_2}{\partial x^2} - 2ik\sin\alpha\frac{\partial E_2}{\partial x} + k^2(n^2(\theta)-1)E_2\right] \\
N &= 2
\end{aligned}$$

It is simple to extend the stuck to the case of N-general gaussian beams; in normal-

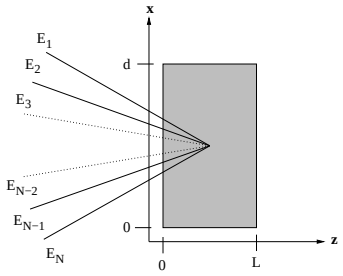

Figure 6: *Rappresentation of the NLC cell acted on by N-gaussian beams*

ized coordinates we obtain like in (35)

$$\begin{aligned}
\frac{\partial\theta}{\partial\tau} &= \nabla^2\theta \qquad + \qquad \left[\sum_{i,j=1}^{N} e_i e_j^* \sin(2\theta - \alpha_i - \alpha_j)\right] \\
\frac{\partial e_1}{\partial\zeta} &= -\frac{i}{\Xi\cos\alpha}\left[\frac{\partial^2 e_1}{\partial\xi^2} - i\Xi\sin\alpha\frac{\partial e_1}{\partial\xi} + \Xi^2\eta(\theta)e_1\right] \\
\frac{\partial e_2}{\partial\zeta} &= -\frac{i}{\Xi\cos\alpha}\left[\frac{\partial^2 e_2}{\partial\xi^2} - i\Xi\sin\alpha\frac{\partial e_2}{\partial\xi} + \Xi^2\eta(\theta)e_2\right] \\
&\vdots \\
\frac{\partial e_N}{\partial\zeta} &= -\frac{i}{\Xi\cos\alpha}\left[\frac{\partial^2 e_N}{\partial\xi^2} - i\Xi\sin\alpha\frac{\partial e_N}{\partial\xi} + \Xi^2\eta(\theta)e_N\right]
\end{aligned} \tag{35}$$

where

$$\begin{aligned}
\xi &= x/L; & \zeta &= z/L; \\
\tau &= t/\tau_r; & \tau_r &= K/L^2\gamma; \\
e_i &= \sqrt{\Delta\varepsilon\varepsilon_0}E_i/2; & \Xi &= 2Lk; \\
\eta(\theta) &= (n^2(\theta) - 1)/4 & i &= 1,\ldots,N
\end{aligned}$$

System (35) has been solved by using a numerica approach. Since in order to study the effect of CAW or LIFT II the interference term in Frank's equation (30) can be neglected; therefore to decrease the computational time, we have utilized only the gaussian beams propagating in the cell. On the contrary for Light charges and other non-local phenomena, was necessary to include the interference term and then the computational time increase.

Boundary conditions are:

- the cell is homeotropically aligned that means $\theta(\xi,\zeta,0) = 0 \qquad \forall\xi,\zeta$;
- there are strong anchoring conditiosn that means $\theta(\xi,0,\tau) = \theta(\xi,1,\tau) = 0 \qquad \forall\xi,\tau$;

- impinging beams $e_i(\xi, 0, \tau), e_2(\xi, 0, \tau), \ldots, e_N(\xi, 0, \tau)$ have a gaussian profile.

Then we have used the Runge-Kutta method for solving the temporal derivative and the central difference method for the spatial derivative. The flow chart reported in Figure 7 rappresents the detail of computational steps:

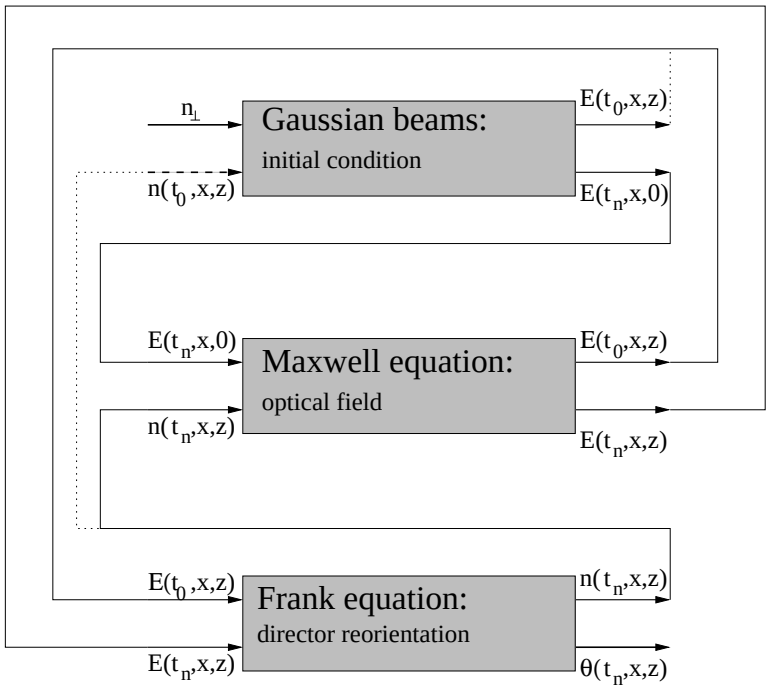

Figure 7: *Flow chart of the numerical code: solid lines rappresent the code solving the system (35), dashed line rappresent the case if we want to neglect the interference term*

In the chapter 1 numerical results of the code and comparisons with experimental measures are reported. Investigation about light charges is work in progress. This argument are reported in papers [12] and [13].

IV.2 Molecular director reorientation and light propagation in liquid crystal cells with multiple interfaces

Spatial solitary waves or solitons have been widely investigated in recent years both for basic research interest and for their potentials in signal processing, optical switching and all-optical readdressing [14–19]. In particular scientists have been searching for suitable optical materials that could support this kind of nonlinear effects. In general, in order to induce nonlinear effects in usual optical materials, pulsed laser sources are needed to comply with high peak power requirements. From this point of view, liquid crystals represent a promising alternative, because of their reorientational optical nonlinearities which can be excited at very low optical intensities, about 100 times lower than in conventional nonlinear materials [20, 21]. In an uniaxial crystal like a nematic liquid crystal (NLC), a spatial soliton can be observed due to the reorientational response that causes a dependence of the refractive index on the optical intensity. When a light beam propagates in such a medium, the refractive index increases in the central, and most intense, region of the beam thus causing a self-focusing effect which can balance linear diffraction [22]. In this case, the beam spot size does not change during propagation and the field distribution represents a particular eigen-solution of the corresponding nonlinear propagation equation. In this scenario, NLCs provide an ideal workbench for investigation of spatial solitons, not only because of the large nonlinearity [20, 21] and high nonlocality [23, 24], but also because of an electro-optic response, which enables a fine control of birefringence and walk-off [25]. While spatial nonlocality allows both propagation of stable solitons in two transverse dimensions and their long-range interactions [24–26], the high orientational birefringence of the medium allows to

create a broadly tunable walk-off as well as redirection of solitons by using an applied voltage bias [25].

All these phenomena have been observed and characterized in suitable NLC cells which have been designed and fabricated ad hoc, in order to control many of the parameters which are responsible of the exploited nonlinear effects.

Indeed, when light propagates in waveguide regime in standard NLC cells, some interface problem arise: the focused Gaussian laser beam inside the cell sees the meniscus to the interface (where the director configuration is unknown) that acts as a lens and diffracts the input beam causing divergence and losses. In order to solve

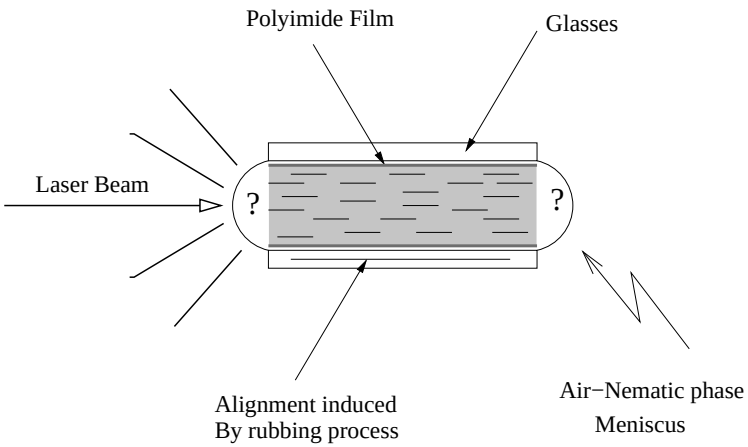

Figure 8: *The unknown configuration of director at the interface produces the scattering of light.*

this problem, the Warenghem group suggested to put inside the cell an optical fibre that crosses the region of unknown configuration as show in Figure 9. This approach eliminates the problem, but gives up to investigate the effect of the interface. Furthemore, as a matter of fact, the study of optical solitons, two wave formation and light filaments steering in liquid crystals requires the utilization of particular cells designed for top view investigation. These are realized with a lateral input interface

that enables to control the molecular director reorientation and prevents light scattering. in this sense, our solution was to put an additional interafce which imposes

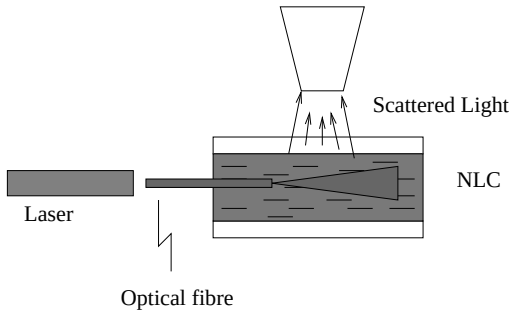

Figure 9: *The Warenghem group suggested to put inside the cell an optical fibre that crosses the region of unknown director orientation and solves the problem due to light scattering*

an easy direction to the molecular director, as show in Figure 10. The laser light

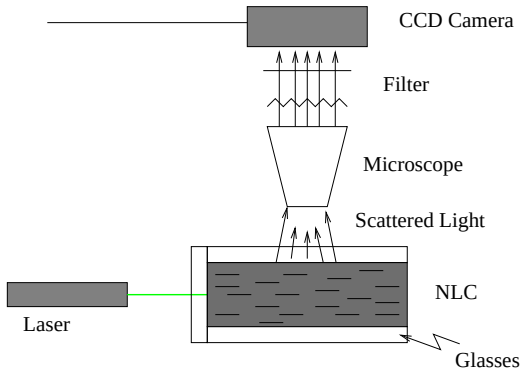

Figure 10: *Our solution was to put an additional interafce imposing an easy direction to the molecular director. The laser light propagates in waveguide regime and the light scattered from the top is collected by a microscope and then elaborated through a CCD camera. The properties of formation, steering and routing of solitons inside this cell depends on the particular rubbing imposed at the additional interface as shown in chapter 3*

propagates in waveguide regime and the light scattered from the top is collected by a microscope and then elaborated through a CCD camera. The formation, steering and routing of solitons inside this cell depend on the particular rubbing imposed at

the additional interface as shown later (chapter 3). The final cell configuration is shown in Figure 11 and details of cell fabrication are reported by De Luca et all in [27]. The thickness of the cell is $75\,\mu m$ while the total lenght is several cm.

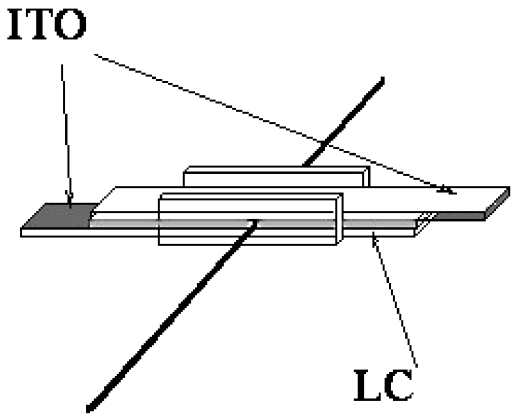

Figure 11: *Sketch of a thin cell with two additional (input and output) optical glass interfaces.*

The self-confinement behavior of a linearly-polarized Gaussian beam is obtained applying an external ac voltage ($f = 1Khz,\ V_{RMS} = 2.3V$).

In order to investigate this cell and the relative fenomena, I have studied and rewritten the equations that describe the system in the most general case, including the energy ancoring at the interface due to the rubbing; in this cese, a numerical approach is needed the reference system the one of Figure 1 but, for computational memory limits the numerical analisys is concetrated in the $x - z$ plane. I have considered both Frank's equations for $\theta(x, z, t)$ and $\phi(x, z, t)$ and two more equations for the two optical field components $E_x(x, z, t)$ and $E_y(x, z, t)$. The variational calculus predicts that, if an additional surface term is added to the energy density, an additional equation is necessary to find the minumum energy, or steady state,

configuration. Then the total equation system is:

$$\frac{\partial\theta}{\partial\tau} = \nabla^2\theta + \sin\theta\cos\theta\ \ \nabla\phi\cdot\nabla\phi + \Big(\sin 2\theta|\mathcal{E}_\xi|^2 - \sin 2\theta\cos^2\phi|\mathcal{E}_\zeta|^2 + \\ + \cos 2\theta\cos\phi\left(\mathcal{E}_\xi\mathcal{E}_\zeta^* + \mathcal{E}_\xi^*\mathcal{E}_\zeta\right)\Big) + \sin 2\theta\mathcal{E}_{LF}^2$$

$$\frac{\partial\phi}{\partial\tau} = \cos^2\theta\nabla^2\phi - \sin 2\theta\ \ \nabla\theta\cdot\nabla\phi - \Big(\cos^2\theta\sin 2\phi|\mathcal{E}_\zeta|^2 + \\ + \sin\theta\cos\theta\sin\phi\left(\mathcal{E}_\xi\mathcal{E}_\zeta^* + \mathcal{E}_\xi^*\mathcal{E}_\zeta\right)\Big)$$

$$\frac{\partial\overrightarrow{\mathcal{E}}}{\partial\zeta} = A\frac{\partial^2\overrightarrow{\mathcal{E}}}{\partial\xi^2} + B(\hat{\varepsilon} - \hat{\varepsilon}_{init})\overrightarrow{\mathcal{E}}$$

taking into account eq. (1) in our reference system

$$\frac{\partial\mathcal{E}_\xi}{\partial\zeta} = A\frac{\partial^2\mathcal{E}_\xi}{\partial\xi^2} + B\Delta\varepsilon\Big[(\sin\theta - \sin\theta_i)\mathcal{E}_\xi \\ + (\sin\theta\cos\theta\cos\phi - \sin\theta_i\cos\theta_i\cos\phi_i)\mathcal{E}_\psi\Big]$$

$$\frac{\partial\mathcal{E}_\psi}{\partial\zeta} = A\frac{\partial^2\mathcal{E}_\psi}{\partial\xi^2} + B\Delta\varepsilon\Big[(\sin\theta\cos\theta\cos\phi - \sin\theta_i\cos\theta_i\cos\phi_i)\mathcal{E}_\xi \\ + (\cos^2\theta\cos^2\phi - \cos^2\theta_i\cos^2\phi_i)\mathcal{E}_\psi\Big]$$

where the normalized variables are:

$$\xi = x/D; \qquad \zeta = z/D; \qquad \tau = t/\tau_r; \qquad \tau_r = K/D^2\gamma;$$
$$\overrightarrow{\mathcal{E}} = \sqrt{\frac{D^2\varepsilon_0\Delta\varepsilon}{4K}}\overrightarrow{E}; \quad \mathcal{E}_{LF} = \sqrt{\frac{D^2\varepsilon_0\Delta\varepsilon_{LF}}{2K}}E_{LF}; \quad A = \frac{1}{2ikD}; \quad B = \frac{k_0D}{2ik}$$
$$k = k_0n_{eff}; \qquad \Delta\varepsilon = \varepsilon_\parallel - \varepsilon_\perp$$

The additional equations to be solved at the three surfaces where the rubbing treatment has been made are reported in the following system. The surfuces with rubbing are defined at the planes $x = 0,\ x = d,\ z = 0$, which in normalized variables, become $\xi = 0,\ \xi = 1,\ \zeta = 0$:

$$\xi = 0 \quad \rightarrow \quad \begin{cases} \frac{\partial\theta}{\partial\xi} & = \frac{DW^{\theta}}{K}\sin(\theta-\theta_i)\cos(\theta-\theta_i) - \cos^2\theta\cos\phi\frac{\partial\phi}{\partial\zeta} \\ \frac{\partial\phi}{\partial\xi} & = \frac{DW^{\phi}}{K\cos^2\theta}\sin(\phi-\phi_i)\cos(\phi-\phi_i) + \cos\phi\frac{\partial\theta}{\partial\zeta} \end{cases}$$

$$\xi = 1 \quad \rightarrow \quad \begin{cases} \frac{\partial\theta}{\partial\xi} & = -\frac{DW^{\theta}}{K}\sin(\theta-\theta_i)\cos(\theta-\theta_i) - \cos^2\theta\cos\phi\frac{\partial\phi}{\partial\zeta} \\ \frac{\partial\phi}{\partial\xi} & = -\frac{DW^{\phi}}{K\cos^2\theta}\sin(\phi-\phi_i)\cos(\phi-\phi_i) + \cos\phi\frac{\partial\theta}{\partial\zeta} \end{cases}$$

$$\zeta = 0 \quad \rightarrow \quad \begin{cases} \frac{\partial\theta}{\partial\zeta} & = \frac{DW^{\theta}}{K}\sin(\theta-\theta_i)\cos(\theta-\theta_i) + \cos^2\theta\cos\phi\frac{\partial\phi}{\partial\xi} \\ \frac{\partial\phi}{\partial\zeta} & = \frac{DW^{\phi}}{K\cos^2\theta}\sin(\phi-\phi_i)\cos(\phi-\phi_i) - \cos\phi\frac{\partial\theta}{\partial\xi} \end{cases}$$

In order to numerically solve this complex equation system I had to implement a code flow chart more complex then the previous one. In this case, indeed, there are two intial conditions: the first one is the director orientation at $t = 0$ (we have to know $\theta(\xi, \zeta, 0)$ and $\phi(\xi, \zeta, 0)$ in each point of the $x - z$ plane); the second one is the input profile of beam, (we send a gaussian beam). When these two initial configurations are know, two subroutines elaborate the field value and the angle values in each point of the $x - z$ plane, at each time instant.

In order to realize this code, I have realized and tested separatly the two codes that constitute the two subroutines.

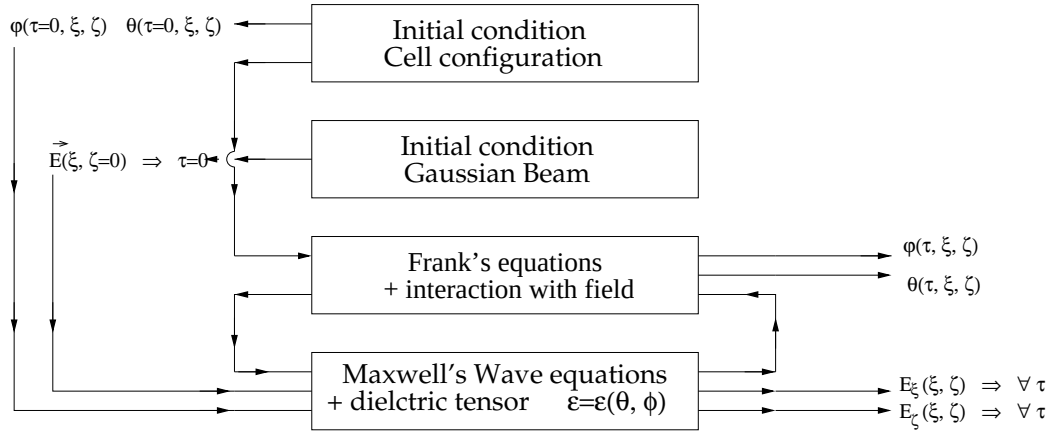

Figure 12: *Code flow chart: there are two initial conditions (one for the cell configuration $\theta(\xi, \zeta, 0)$, $\phi(\xi, \zeta, 0)$, one for the beam gaussian profile) and two subroutine that elaborate the field value $\mathcal{E}(\xi, \zeta)$ the new angle values at each time instant.*

IV.2.1 Periodic and non periodic potential

The subroutine for the beam propagation is quite similar to the one of the previous code; the best form is:

$$\frac{\partial \mathbf{E}}{\partial \zeta} + \frac{i}{2\tilde{k}_z}\frac{\partial^2 \mathbf{E}}{\partial \xi^2} + \frac{\tilde{k}_x}{\tilde{k}_z}\frac{\partial \mathbf{E}}{\partial \xi} + \frac{i\tilde{k}_0^2}{2\tilde{k}_z}\left[n^2(\xi) - 1\right]\mathbf{E} = 0$$

where the normalized variables are:

$$D = 100\mu m \qquad \text{(normalization lenght)}$$

$$\tilde{k}_x = Dk\sin\alpha; \qquad \tilde{k}_z = Dk\cos\alpha;$$

$$\tilde{k}_0 = \frac{2\pi D}{\lambda} \qquad k = \frac{2\pi n[\xi]}{\lambda}$$

$$\xi = x/D; \qquad \zeta = z/D;$$

$$n(\xi) = \qquad \text{refractive index}$$

I have tested the subroutine for periodic and non periodic potentials, obtaining the new results reported in chapter 2.

IV.2.2 Cell configuration

The subroutine for the cell configuration requires an initial condition that corresponds to the steady state with the particular rubbing that we want to take into account. Therefore, we have to solve in advance the steady state Frank equations:

$$\nabla^2\theta + \sin\theta\cos\theta \ \ \nabla\phi\cdot\nabla\phi = 0$$

$$\cos^2\theta\nabla^2\phi - \sin 2\theta \ \ \nabla\theta\cdot\nabla\phi = 0$$

where the normalized variables are:

$$D = 75\mu m \qquad \text{(normalization lenght)}$$

$$\xi = x/D;$$

$$\zeta = z/D;$$

$$\tau = t/\tau_r;$$

$$\tau_r = K/D^2\gamma;$$

$$K_1 = K_2 = K_3 = K$$

Results related to the three particular configuration that have been experimentally investigated are in good agreement with experimental results and are reported in chapter 3.

Bibliography

[1] F. C. Frank, *Discuss. Faraday Soc.***25**, 19 (1958).

[2] E. Fermi, *Termodinamica* Boringieri, Torino (1968)

[3] I. C. Khoo, F. Simoni, *Phisics of Liquid Crystalline Materials* Gordon and Breach, Philadelphia (1991)

[4] L. M. Blinov, A. Yu. Kabayenkov, and A. A. Sonin, *Liquid Crystals* **5**, 645 (1989)

[5] A. Rapini, M. Popular *Jour. de Physique (Coll)* **30 C4**, 54 (1969)

[6] B. Ya Zel'dovich, N. V. Tabiryan *Sov. Phys. JEPT* **55**, 656 (1982)

[7] P. Kaczmarski, P. E. Lagasse, *Electron. Lett.* **24**, 675 (1988)

[8] G. H. Jin, J. Harari, J. P. Vilcot, D. Decoster, *Electron. Lett.* **31**, 1867 (1995)

[9] M. Born and K. Huang. *Dynamical Theory of Crystal Lattices* Oxford University Press, Oxford, (1954)

[10] D. N. Christodoulides and R. I. Joseph. *Opt. Lett.*, **13**: 794–796, (1988)

[11] Charles Kittel *Introduction to solid state physics* New York, (1996)

[12] Veltri A. , **Pezzi L.** , De Luca A. , Umeton C. P. *"Different reorientational regimes in a liquid crystalline medium undergoing multiple irradiation"* **Optics Express**, 2007, Vol. 15, n. 4, pp. 1663-1671

[13] **Pezzi L.**; A. Veltri; A. De Luca; C. Umeton *"Non-Linear Effects in NLC Media Undergoing Two Beams Irradiation"* **MCLC** Molecular Crystals and Liquid Crystals; April 2007; Volume 465 No. 1 Pages 71 - 80

[14] G. I. Stegeman and M. Segev, *Optical Spatial Solitons and Their Interactions: Universality and Diversity,* **Science** 286, 1518 (1999)

[15] G. Stegeman, D. Christodoulides, and M. Segev, *Optical spatial solitons: historical perspectives,* **IEEE J. Sel. Top. Quantum Electron.** 6, 1419 (2000)

[16] A. D. Boardman and A. P. Sukhorukov *Soliton Driven Photonics* (Kluwer, Dordrecht, 2001)

[17] S. Trillo and W.E. Torruellas, *Spatial Solitons* (Springer-Verlag, Berlin, 2001)

[18] Y. Kivhsar and G. Agrawal, *Optical Solitons: From Fibers to Photonic Crystals* (Academic Press, London, 2003)

[19] C. Conti, M. Peccianti, and G. Assanto, Observation of Optical Spatial Solitons in a Highly Nonlocal Medium, Phys. Rev. Lett. 92, 113902 (2004)

[20] N. V. Tabyrian, A.V. Sukhov, and B.Y. Zeldovich, *The orientational optical nonlinearity of liquid crystals,* **Mol. Cryst. Liq. Cryst.** 136, 1 (1986)

[21] I. C. Khoo, *Liquid Crystals: Physical Properties and Nonlinear Optical Phenomena* (Wiley, New York, 1995)

[22] M. Segev and G. I. Stegeman, *Self-Trapping of Optical Beams: Spatial Solitons,* **Phys. Today** 51, 42 (1998)

[23] C. Conti, M. Peccianti, and G. Assanto, *Route to Nonlocality and Observation of Accessible Solitons,* **Phys. Rev. Lett.** 91, 073901 (2003)

[24] M. Peccianti, K. A. Brzadkiewicz, and G. Assanto, *Nonlocal spatial soliton interactions in nematic liquid crystals,* **Opt. Lett.** 27, 1460 (2002)

[25] M. Peccianti, C. Conti, G. Assanto, A. De Luca, and C. Umeton, *Routing of anisotropic spatial solitons and modulational instability in liquid crystals,* **Nature** 432, 733 (2004)

[26] B.B. Kosmowski, M.E. Becker, and D.A. Mlynski, *A novel technique for the accurate determination of average tilt angle in twisted nematic cells,* **Displays** 5, 104 (1984)

[27] A. De Luca, G. Coschignano, M. Morabito, C.P. Umeton, Optics Express **14**(12), 5548 (2006)

Chapter 1

Reorientational effects undergoing multiple irradiation

We present a numerical approach to the nemato-elasticity differential equation in a nematic liquid crystal cell when irradiated with multiple gaussian beams. Solutions have been carried out on a configuration with two coplanar beams illuminating the sample in order to compare it with particular nonlinear phenomena experimentally studied in the past. A new set of experimental measures were realized confirming the validity of the numerical model. Solutions for an instable case showing nonlocal effects are also presented as an example of the broader class of systems this approach can describe.

1.1 Introduction

Light propagation in nematic liquid crystals (NLC) and the consequent self-induced effects are, by definition, the basics of nonlinear optics in such materials. In this perspective, orientational interaction phenomena have been widely studied during last two decades, providing a great number of fundamental and applied results [1–3]. In recent years, other nonlinear media have been deeply investigated to time domain phenomena [4, 5], spatial effects in photorefractive materials [6, 7] and spatial optical solitons, intended as non-diffracting light beams that are self-confined by the nonlinearity. Because of their possible applications (related to the exploitation of the wave-guiding character [8]), spatial optical solitons have been intensely investigated also in a new scenario, which describes these effects in a smooth transition from the purely local to the entirely nonlocal response [9]. In that case, the physical system was again a nematic liquid crystal in a planar cell exhibiting a nonlocal nonlinearity of orientational molecular origin [2], which had already been used for the observation of $(2+1)$D spatial solitons [10]. Furthermore, it has been shown that different solitons created in the same sample by different light beams can interact each other giving rise to a series of interesting effects and leading to intriguing applications like the realization of logic gates [10]. Recently [12], it has been found that the possibility of a nonlinear interaction between different light beams is not limited to the case of spatial solitons, but can take place also in different experimental conditions, giving rise to a series of intriguing effects. In particular, it has been found that the nonlinear response induced by one beam can be partially or totally cancelled by a second beam, with interesting perspectives for possible applications. In this perspective, however, further investigations and availability of a

general and complete theoretical description for the interpretation of these effects are mandatory if their application oriented utilization is desired. We present a general model which describes the behavior of a highly nonlinear system like a liquid crystal sample when undergoing multiple irradiation; furthermore, we show that, under particular experimental conditions, also nonlocality plays an important role.

1.2 Experiment

The Giant Optical Nonlinearity (GON) of Nematic Liquid Crystals (NLCs) determines important and useful optical properties of these materials [2, 3]. This nonlinearity is due to the reorientation of the molecular director **n**, which is the unit vector that describes the mean orientation of the axis of the elongated NLC molecules [1]. As this vector explicitly appears in the terms that describe the interaction with an external electric field, it happens that the reorientation can be also induced by the optical field of the same radiation that experiences the nonlinear propagation. This phenomenon is called Optical Fredericksz Transition (OFT), and its most spectacular consequence is the self-phase modulation (SPM) effect, which yields the appearance of concentric bright and dark rings [13] in the far-field zone. The effect, which has been extensively studied and characterized [16, 17], is of continuing interest because of its appealing applications, both in pure NLC [11, 19] and in liquid-crystalline composite materials [20]. In a previous paper [12] the observation of a new kind of OFT induced in a NLC cell by two pulsed laser beams has been reported. It has been predicted that the director reorientation induced by one electromagnetic wave can be canceled by a second, competing, wave of suitable intensity and angle of incidence [21, 22]. The effect can be achieved only in

a limited range of incidence angle and intensity: above a given intensity threshold, cancellation becomes unstable and a second, Light-Induced, Fredericksz Transition (LIFT II) takes place. Investigation of the whole phenomenon is quite interesting, mainly for those applications in which the GON that is due to the OFT is exploited to create spatial solitons in NLCs [11, 19]. In that case both cancellation and LIFT II effect can play crucial roles when multiple spatial solitary waves are allowed to interact with one another and produce all-optical switching and logic gating in NLC cells [10]. We report a new set of experimental observations as well as a theoretical model which describes this phenomenon.

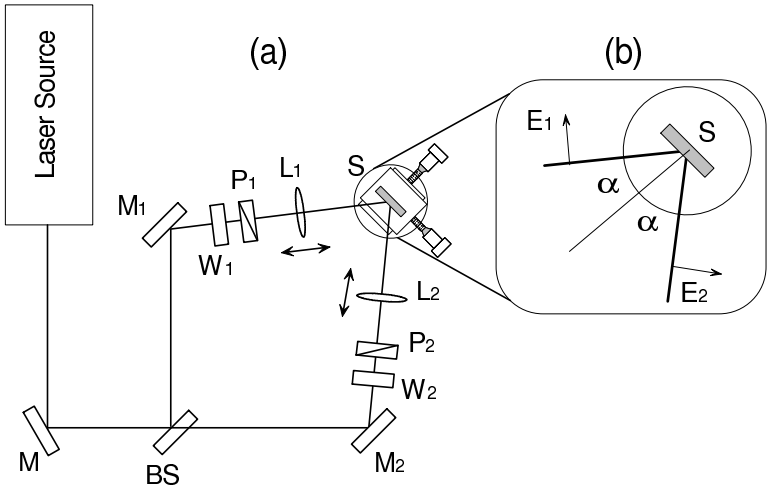

Figure 1.1: *(a) Setup: W, λ/2 plate; Ps polarizers; Ms, mirrors; B.S., 50% beam splitter; CC, corner-cube retroreflector; Ls, lenses; S, sample; SC, screen. (b) Experimental geometry.*

The experimental geometry is illustrated in Fig.1.1. We exploit a particular set of cancellation conditions [16]:The average intensities of the two impinging beams are the same, and the two angles of incidence are equal. The setup is shown in Fig. 1.1(a). The continuous source is a diode-pumped solid-state laser (DPSS Ventus

532, by Laser Quantum) which emits light at λ = 532 nm. The radiation is split into two beams of equal intensity by a beam splitter. Before reaching the sample, each beam crosses a half-wave plate followed by a polarizer, whose combined action enables varying the total power on the sample; then each beam crosses a spherical lens (f = 150 mm), mounted on a translation stage, needed to have two equal spot sizes (130 μm in diameter) on the sample. The NLC (E7, by Merck) is sandwiched between two glass slabs and is homeotropically aligned. Suitable Mylar spacers ensure a uniform thickness (L = 75 μm) of the cell, which is placed on a rotating xyz stage, needed to adjust two equal and opposite angles of incidence. Images after the sample are projected onto a white screen which enables observation of Self Phase Modulation (SPM) rings in the far-field zone, an effect widely investigated in the past [15, 17], which can be used to monitor the director reorientation.

Using an angle of 50^o between the beams, we can obtain a well-balanced competition of the two extraordinary waves. Indeed, when their intensity is the same and the total average intensity on the sample remains below the LIFT II threshold, we obtain an unperturbed orientational state of the director, which we refer to as spatial cancellation of the reorientation. The situation is shown in Fig. 1.2(a), where no SPM rings are observed in the far field zone. If we stop one beam, the action of the other one gives rise to the formation of four SPM rings [Fig. 1.2(b)].

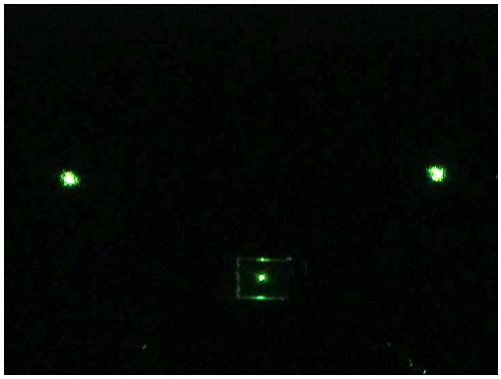

(a)

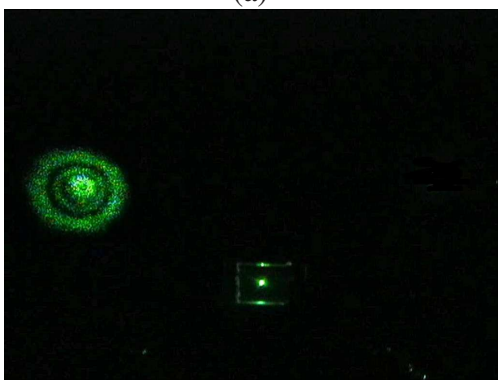

(b)

Figure 1.2: *(a) Cancellation effect. The presence of two dotlike spots shows that there is no nonlinear phase shift. (b) Starting from the previous cancellation state, typical self-phase-modulation rings (which are due to director reorientation) are observed in the far-field zone of the first beam when the second beam is stopped. The impinging intensity of the first beam is the same as in (a).*

When the total impinging intensity reaches the threshold value, a LIFT II effect takes place. The formation of more than 15 SPM rings in the far-field zone of one of the two beams (Fig. 1.3) emphasizes that we are in the presence of a new reorientation of the director in the (x, z) plane. Furthermore, if we stop the beam that exhibits the smallest divergence (first beam), we observe a decrease in the divergence of the second beam. However, if we stop the second beam, we observe a decrease in the divergence of the first beam, followed by the formation of a new ring pattern.

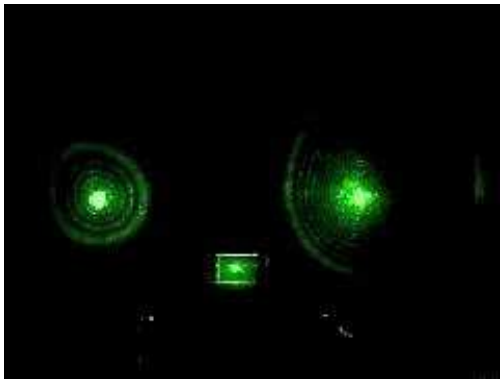

Figure 1.3: *Self-phase-modulation rings that appear in the far-field zone of both beams when the total impinging intensity exceeds the threshold value of the LIFT II effect.*

1.3 Theoretical model

The physical quantities playing the main roles are the re-orientation angle θ of the NLC molecular director $\hat{\mathbf{n}}$ (the unit vector which describes the mean orientation of molecular axes) with respect to the initial (or steady state) direction and the polarization of the impinging light beams. The system we want to study is, in fact the one presented in fig 1.4: a NLC cell of thickness L, and width d, crossed by N laser beams with electric field E_j $(j = 1, \ldots, N)$ and wavelength λ, linearly polarized in the xz-plane, each of them impinging on the sample with an incidence angle α_j. As for system coordinates, we chose the x-axis along the cell width and the z-axis along the cell length. In fact, even if gaussian beams are three-dimensional, the utilization of beams that are linearly polarized in the xz-plane allow to describe all the physics by considering only two dimensions. For sake of generality, we start from the master equation for the angle θ in the case of N reorienting light beams [13]:

$$\gamma \frac{\partial \theta}{\partial t} = \mathcal{K} \nabla^2 \theta + \frac{\varepsilon_0 \Delta\varepsilon}{4} \sum_{i,j=1}^{N} E_i E_j^* \sin(2\theta - \alpha_i - \alpha_j), \tag{1.1}$$

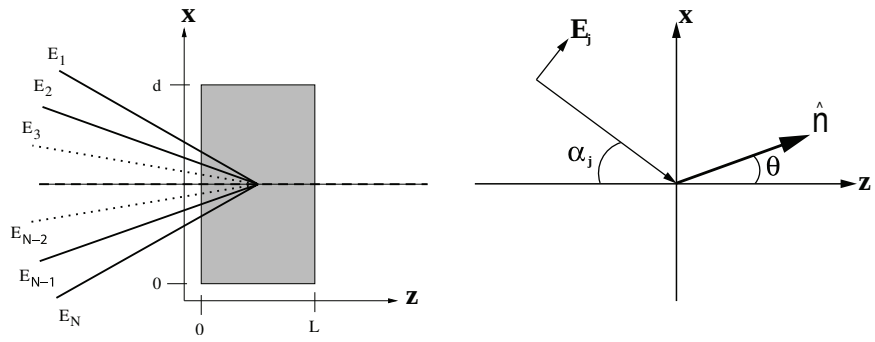

Figure 1.4: *Here we represent the system under study that is an NLC cell of tickness L, and width d, crossed by E_j ($j = 1, \ldots, N$) gaussian light beams, each of them impinging on the sample with angle α_j. The director orientation is identified by the angle θ formed by the director $\hat{n}$ and the z-axis*

where t is the time, γ the viscosity constant and $\mathcal{K}$ the elastic constant of the medium in a "one constant" approximation [13]; $\Delta\varepsilon = n_e^2 - n_o^2$ indicates the optical anisotropy, n_e and n_o being the extraordinary and ordinary refractive index respectively; ε_0 is the electric permittivity of vacuum.

Where light propagation is concerned, considering that investigated phenomena occur in a small fraction of a thin cell, we use the fundamental gaussian beam solution of Maxwell equations [14] instead of solving a new light propagation equation, taking into account that the j-th beam crosses the sample with an angle α_j; this corresponds to apply the following transformation on the solution propagating along z:

$$\begin{aligned} x &\longrightarrow x\cos\alpha_j - z\sin\alpha_j \\ z &\longrightarrow x\sin\alpha_j + z\cos\alpha_j \end{aligned} \tag{1.2}$$

While crossing the medium the j-th beam experiences a refractive index $n(\alpha_j, \theta)$ given by [2]:

$$n(\alpha_j, \theta) = \frac{n_o n_e}{\sqrt{n_e^2\cos^2(\alpha_j - \theta) + n_o^2\sin^2(\alpha_j - \theta)}}. \tag{1.3}$$

Where θ is obtained from the solution of equation (1.1). We introduce normalized coordinates $\xi = x/L$, $\zeta = z/L$ and normalized time $\tau = t/\tau_R$, where $\tau_R = \gamma L^2/\mathcal{K}$ is the tipical reorientation time of the NLC director [2]. We also introduce parameters $\Lambda = \lambda/L$, which is the normalized wavelength and $w_0 = W_0/L$ which is a normalized minimum spot size (W_0 being the minimum spot size), and a normalized expression for the electric field: $e_j = E_j\sqrt{L^2\varepsilon_0\Delta\varepsilon/4\mathcal{K}}$.

Thus, the normalized electric field of the j-th gaussian beam is written as:

$$e_j = \frac{e_0 w_0}{w_j}\exp\Bigg\{-i\big[k(\xi\sin\alpha_j + \zeta\cos\alpha_j) - \eta_j\big] - (\xi\cos\alpha_j - \zeta\sin\alpha_j)^2\left[\frac{1}{w_j^2} + \frac{ik}{2r_j}\right]\Bigg\}$$

$$j = 1, ...N$$

Here $e_0 = E_0\sqrt{L^2\varepsilon_0\Delta\varepsilon/4\mathcal{K}}$ (where E_0 is the field amplitude), $\eta_j = \eta(\zeta, \alpha_j)$, $w_j = W(\zeta, \alpha_j, w_0)$ and $r_j = R(\zeta, \alpha_j)$, where $W(z) = W_0\sqrt{1 + z^2/z_0^2}$ is the spot size, $z_0 = \pi n(\theta)W_0^2/\lambda$ the confocal parameter, $\eta(z) = \arctan(z/z_0)$ and $R(z) = z + z_0^2/z$ is the radius of curvature of a generic gaussian beam. In normalized coordinates, equation (1.1) becomes:

$$\frac{\partial\theta}{\partial\tau} = \nabla^2\theta + \sum_{i,j=1}^{N} e_i e_j^* \sin(2\theta - \alpha_i - \alpha_j), \tag{1.4}$$

where ∇^2 indicates now $(\partial^2/\partial\xi^2 + \partial^2/\partial\zeta^2)$.

1.4 Numerical solutions and results

Equation 1.4 can be used to study a large number of experimental configurations, but it is highly nonlinear and, in general, cannot be solved by analytical methods. We have chosen a numerical approach by developing a c++ code compiled under Linux using the open source GNU compiler gcc 3.3.5. In particular we have used a second order Runge Kutta time scheme and a central difference scheme for spatial derivatives. We have created a lattice of computational grid points (i, j) in the x-z plane, where lattice steps Δx and Δz allow to go from i to $i + 1$ and from j to $j + 1$ respectively. Evolution of the optical field in the z direction is then simulated by determining the value of the field at the $(i, j + 1)$ point by means of the field values at previous points. The lattice also evolve in time with Δt steps, taking into account the time-dependent molecular director reorentation. In order to test our model a number of simulations have been carried out reproducing experimental configuration presented in [12] that is: utilizing $n_o = 1.5216$ and $n_e = 1.7462$, corresponding to values of the $E7$ commercial NLC, $\lambda = 532$ nm, considering two beams of equal intensity, and using $\theta(\xi, \zeta, 0) = 0$ as the initial condition in time and $\theta(\xi, 0, \tau) = \theta(\xi, 1, \tau) = 0$ as boundary conditions in space; this accounts for strong anchoring in a homeotropic cell, were the molecular director is oriented perpendicularly to the cell plates. As in [12], at first only one beam crosses the sample, so that a director reorientation is induced. The system proceeds this way until $\partial\theta_c/\partial\tau \leq 0.01$, where θ_c indicates the reorientation angle in the center of the sample; then the second beam is switched on at the symmetric incident angle ($\alpha_1 = -\alpha_2$), again until $\partial\theta_c/\partial\tau \leq 0.01$. After that, two different behaviors can be observed (in agreement with experimental results presented in [12]), depending both on light intensity and incidence angle:

1. CAW (Competingly Acting Waves): The second beam competes with the first one and the final effect is a reorganization of the NLC director in such a way that the reorientation effect produced by the first beam is almost completely cancelled by the second one, as presented in fig. 1.5; a plot of simulated

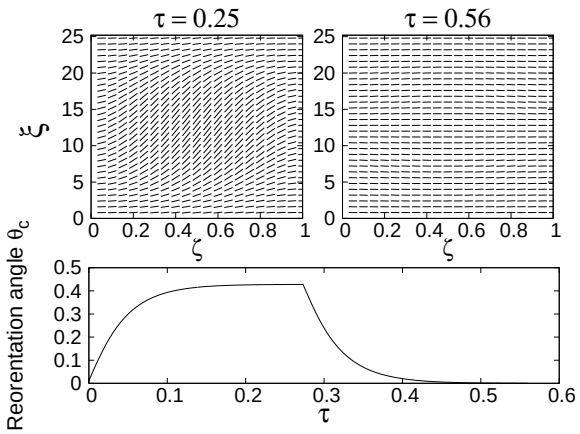

Figure 1.5: *Simulation carried out for an angle of incidence* $\alpha = 1$ *rad and a normalized field amplitude* $e_0 = 3$*. The first and second frames show the orientation of the molecular director in the sample at* $\tau = 0.25$*, and* $\tau = 0.56$*; the third is the temporal behavior of the reorientation angle* θ_c *in the center of the sample. This case represents a complete cancellation effect induced by the competition of the two beams.*

refractive index profile is reported in the following Fig. 1.6.

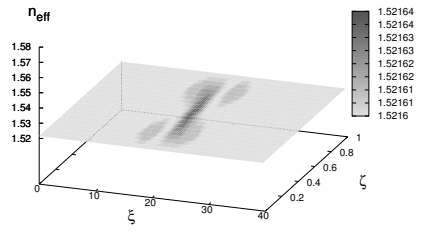

Figure 1.6: *Plot of simulated refractive index profile in the normalized* $\xi - \zeta$*-plane in CAW condition with* $\alpha = 0.1$ *rad,* $e_0 = 3$ *at* $\tau = 0.56$

2. LIFT II (Second Light Induced Fréedericksz Transition): above a given in-

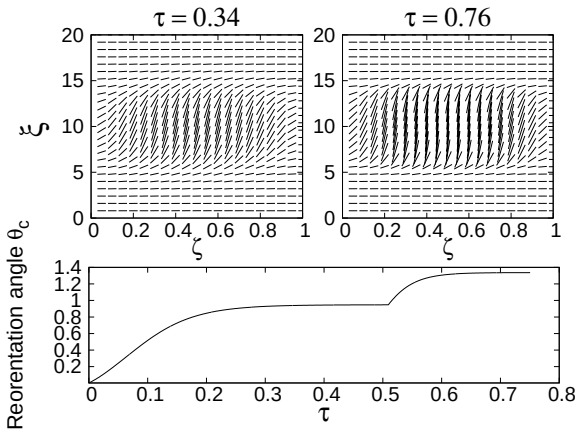

Figure 1.7: *Simulation carried out for* $\alpha = 0.2$ *rad,* $e_0 = 3$*. The first and second frames show the orientation of the molecular director in the sample at* $\tau = 0.34$*, and* $\tau = 0.76$*; the third is the temporal behavior of the reorientation angle* θ_c *in the center of the sample. This case represents a critical reorientation effect due to the second light-induced Fréedericksz transition (LIFT II)*

tensity threshold, the second beam adds its reorientational effect to the first one, thus causing a critical director reorientation (fig. 1.7); a plot of simulated refractive index profile is reported in the following Fig. 1.8.

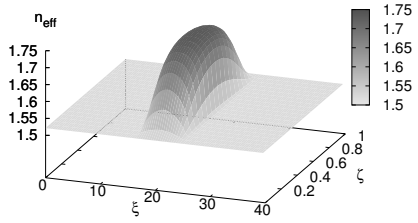

Figure 1.8: *Plot of simulated refractive index profile in the normalized* $\xi - \zeta$*-plane in LIFT II condition with* $\alpha = 0.2$ *rad,* $e_0 = 3$ *at* $\tau = 0.76$

In order to characterize effects of the field amplitude e_0 and incidence angle α_j, we have evaluated the L^2-Norm of $\theta(\xi, 1/2)$, defined as

$$L^2[\theta(\xi, 1/2)] = [\int (\theta(\xi, 1/2))^2 d\xi]^{1/2} \tag{1.5}$$

This quantity is ~ 0 if cancellation occurs, while it is different from zero in the case of critical reorientation. Results of this characterization are presented in fig.1.9:

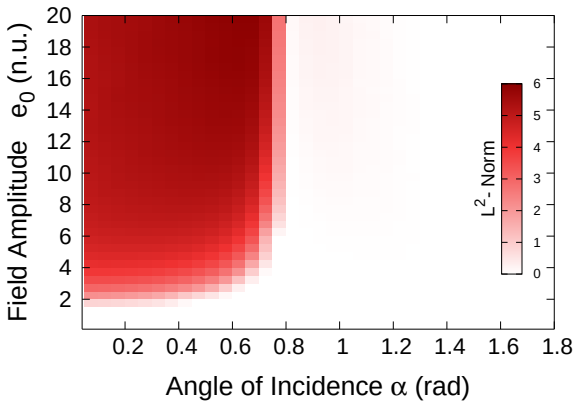

Figure 1.9: *The L^2-Norm of a cut in ξ of $\theta(\xi, \zeta)$ at the center of the sample ($\zeta = 1/2$), as a function of the control parameters e_0 and α, is presented as a measure of the director reorientation. The dark zone corresponds to a critical reorientation, the white one to a cancellation effect. The map refers to the case in which the second beam is switched on the sample well after the reorientation process induced by the first one has been completed.*

The critical reorientation occurs only for angles of incidence smaller than the critical value $\alpha_{th} \simeq 0.8$ rad, which is independent of the used liquid crystal, and is specific of the system geometry only. For equal intensities of the two beams, two equilibrium states exist, as shown in fig. 1.10:

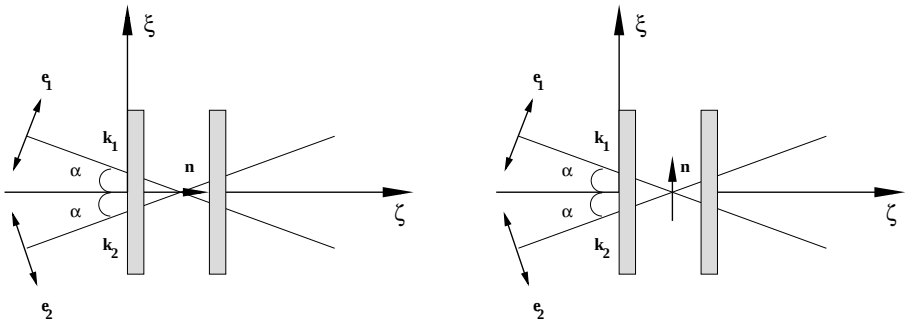

Figure 1.10: *Equilibrium states in the case of equal impinging intensities; vectors* $\mathbf{e}_{1,2}$ *represent the electric fields of light beams,* $\mathbf{n}$ *is the molecular director. (a) initial homeotropic state, or consequence of a complete cancellation effect. (b) complete planar reorientation.*

At great incidence angles ($\alpha > 0.78$ rad, corresponding to small angles between field vectors $\mathbf{e_1}$ and $\mathbf{e_2}$, calculated as $2(\pi - \alpha)$) the cancellation effect is favored; on the contrary, for small incidence angles ($\alpha < 0.78$ rad) a critical reorientation occurs. Furthermore, for values $e_0 < 2$, the reorienting effect is well balanced by the elastic force; the maximum reorientation angle is small enough and the cancellation effect is in any case favored.

1.5 Experimental comparison

Theoretical predictions have been confirmed by experimental results obtained in the geometry illustrated in fig. 1.1(b), which exploits a particular set of conditions: Average intensities of the two impinging beams are the same, whereas the two angles of incidence are equal and opposite. The scheme of the experimental setup is shown in fig. 1.1(a). The continuous source is a diode-pumped solid-state laser (DPSS Ventus 532, by Laser Quantum), which emits light at $\lambda = 532$ nm. The radiation is split into two beams of equal intensity by a beam splitter. Before reaching the sample, each beam crosses a half-wave plate followed by a polarizer, whose combined action enables varying the total power impinging on the sample; then each beam crosses a spherical lens ($f = 150$ mm) mounted on a translation stage, which allows production of two equal spot sizes (~ 130 μm in diameter) on the sample. In this way, two equal light intensities impinge on it. The NLC (E7, by Merck) is sandwiched between two glass slabs and is homeotropically aligned. Suitable Mylar spacers ensure a uniform thickness ($L = 75$ μm) of the cell, which is placed on a rotating xyz stage, needed to adjust two equal and opposite angles of incidence. Images after the sample are projected onto a white screen which enables observation of Self Phase Modulation (SPM) rings in the far-field zone, an effect widely investigated in the past [15, 17, 18], which can be used to monitor the director reorientation. By varying the incidence angle between 20° and 70°, with steps of 10°, we have characterized the dependence of the ring interference pattern on the impinging power. For angles smaller than 45° (0.78 rad) it is possible to obtain a well-balanced competition of the effects of the two beams. Indeed, when their intensities are equal and the total average intensity remains below a given threshold,

SPM rings disappear, indicating an unperturbed orientational state of the director, which we refer to as “spatial cancellation of reorientation”.

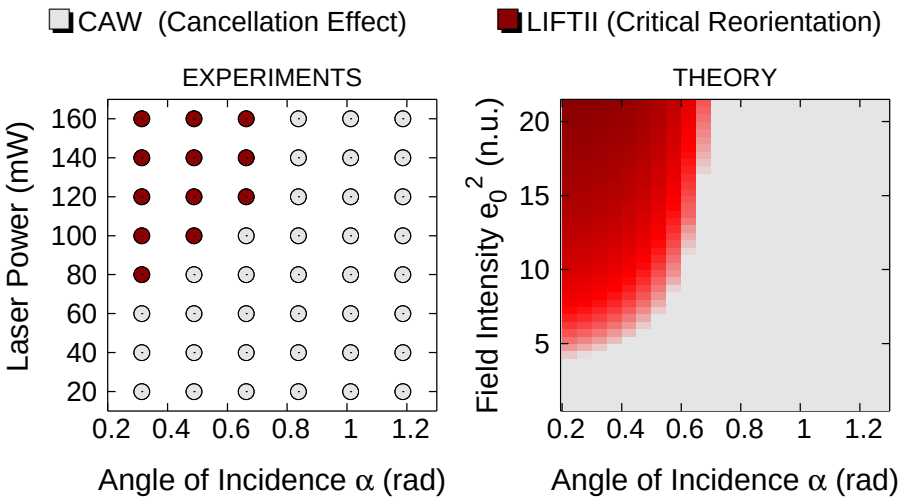

(a) (b)

Figure 1.11: *(a) Experimental results obtained for different values of impinging power and angles of incidence. Black dots indicate that, at the end of the process, reorientation due to a LIFT II effect has taken place. Gray dots indicate that a a complete cancellation has occurred. (b) Theoretical map of* $L^2[\theta(\xi, 1/2)]$ *in the corresponding zone of the* α *-* e_0^2 *plane*

The situation is shown in fig. 1.11(a), where we have used gray dots to refer to the case of no SPM rings observed in the far field zone (45 cm from the sample), while with black dots we have indicated the case of a LIFT II effect. We have chosen to use a field intensity representation for the L^2-Norm values in order to maintain a proportionality with the impinging laser power; normalization relations indicate that the $[0 : 21.6]$ range for e_0^2 corresponds to the $[0 : 160$ mW$]$ range for the laser power.

In fig. 1.11(b) theoretical predictions are reported for the same cases. Also in

this figure the gray zone refers to the case in which a cancellation of reorientational effects is obtained, while the black zone refers to a critical reorientational effect. Comparison with 1.11(a) demonstrates the validity of our model.

Starting from evidences of fig. 1.11, for a deeper investigation of the obtained results, an analysis of the optical divergence of one beam as a function of the impinging laser power has been realized for $\alpha = 0.35$, $\alpha = 0.55$ and $\alpha = 0.65$ corresponding to the appearing of the LIFT II effect. In fact, $L^2[\theta(\xi, 1/2)]$ is a mea-

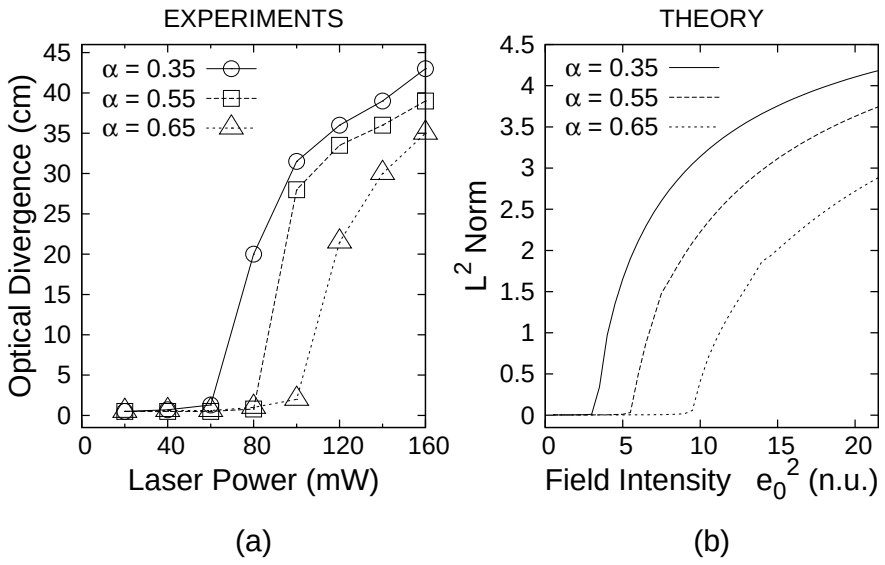

Figure 1.12: *(a) Experimental behavior of the optical divergence as a function of the laser power for different α values that correspond to geometries in which a threshold in the field amplitude exists for the reorientation effect. (b) $L^2[\theta(\xi, 1/2)]$ as a function of e_0^2 (in the corresponding range of values of the field intensity) for the same α values.*

sure of the reorientational effect; on the other hand, the optical divergence of one beam is a direct evidence of the director reorientation [13]. In fig. 1.12(a) the optical divergence as a function of the laser power is reported, while fig. 1.12(b) represents

the theoretical behavior of the L^2-Norm obtained for the same α values in the corresponding range of field intensity. Also in this case, the excellent agreement between the two figures confirms the validity of our model.

1.6 Non local solutions

Effects discussed up to now are concerned with a local responce of the medium and they can be explained by considering the local equilibrium states presented in fig 1.10; there is however a particular case in which nonlocality plays a role. In particular, if both laser beams are switched on the sample simultaneously, an apparently stable situation is realized. On the contrary, theoretical simulations show that a different kind of critical reorientation is observed, due to a nonlocal response of the medium. Indeed, characterization of the L^2-Norm presented in fig. 1.13 shows that also in this case there is a threshold in e_0 and α above which a critical reorien-

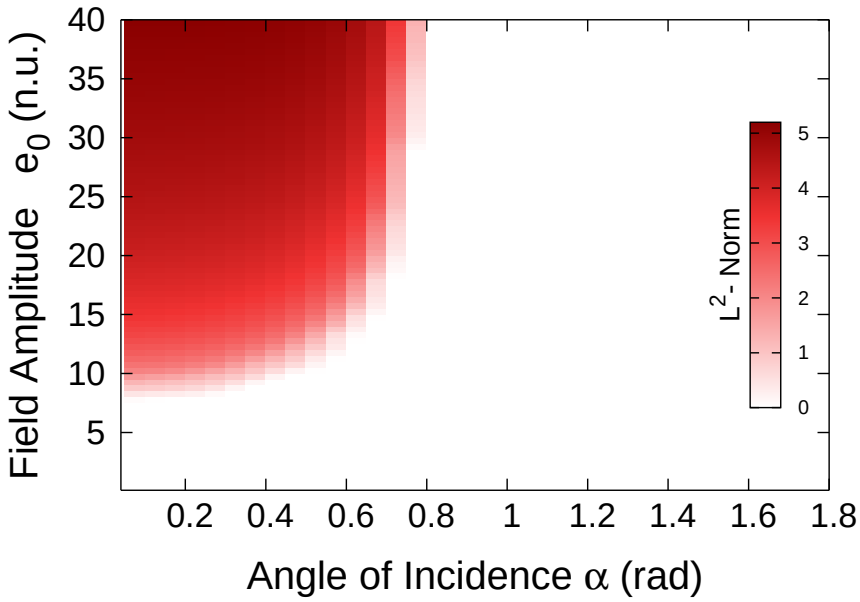

Figure 1.13: *The L^2-Norm of a cut in ξ of θ at the center of the sample ($L^2[\theta(\xi, 1/2)]$), as a function of control parameters e_0 and α. The dark zone corresponds to critical reorientation, the white one to a cancellation effect. The map refers to the case in which the two beams are switched on the sample simultaneously*

tation occurs. In our opinion, this effect can be explained by assuming that, from

the boundary of the irradiated zone where the two gaussian beams are not perfectly superimposed, nonlocality extends the reorientation towards the center of the spot. If elastic forces are relatively small (high e_0), molecules can receive enough energy to evolve from the homeotropic equilibrium state (a in fig. 1.10) to the planar one (b in fig. 1.10). We have called this effect "De-localized Freèderiksz Transition of Second Order" (DELFTII) , which gives evidence of a nonlocal response of the medium. These results show that the interplay between nonlinear and nonlocal effects is an intrinsic feature of the investigated system and open new perspectives for its study not only from a fundamental point of view, but also for applications. In fact, cancellation effects could be utilized in the fields of "optical switching" and "all optical addressing", while the angular dependence of this effect could be exploited in high resolution "optical goniometer" devices.

1.7 Conclusions

In conclusion we have carried out numerical solutions of a general model for the interaction of N gaussian light beams with a physical system which is a NLC cell with strong anchoring conditions. The model has been experimentally checked for the case of two beams in an opposite incidence angle geometry; in good agreement with theoretical predictions, in the framework of a local response of the medium, it has been found that a series of effects can occur. Furthermore, under particular experimental conditions, nonlocality plays an important role.

Acknowledgments

We acknowledge useful discussions in Mathematics with Dr. Luca Guzzardi

Bibliography

[1] P. G. de Gennes, *The physics of liquid crystals* (Clarendon Press, Oxford, 1993).

[2] I. C. Khoo, *Liquid Crystals: Physical Properties and Nonlinear Optical Phenomena* (Jhon Wiley & Sons, Inc., New York, 1995).

[3] F. Simoni, *Nonlinear optical properties of liquid crystals* (World Scientific, 1997).

[4] E. Vanin, A. I. Korytin, A. M. Sergeev, D. Anderson, M. Lisak, and L. Vazquez, *Dissipative optical solitons* Phys. Rev. A **49**, 2806–2811 (1994).

[5] N. N. Akhmediev, M. J. Lederer, and B. Luther-Davis, *Exact localized solution for nonconservative systems with delayed nonlinear response* Phys. Rev. E **57**, 3664–3667 (1998).

[6] S. Abe and A. Ogura, *Solitary waves and their critical behavior in a nonlinear nonlocal medium with power-law response* Phys. Rev. E **57**, 6066–6070 (1998).

[7] E. DelRe, A. Ciattoni, and A. J. Agranat, *Anisotropic charge displacement supporting isolated photorefractive optical needles* Opt. Lett. **26**, 908–910 (2001).

[8] A. D. Boardman and A. P. Sukhorukov, *Soliton Driven Photonics* (Kluwer, Dordrecht, 2001).

[9] C. Conti, M. Peccianti, and G. Assanto, *Observation of Optical Spatial Solitons in a Highly Nonlocal Medium* Phys. Rev. Lett. **92**, 113902–113902 (2004).

[10] M. Peccianti, C. Conti, G. Assanto, A. De Luca, and C. Umeton, *All Optical Switching and Logic Gating with Spatial Solitons in Liquid Crystals* Appl. Phys. Lett. **81**, 3335–3338 (2002).

[11] M. Peccianti, A. De Rossi, G. Assanto, A. De Luca, and C. Umeton, and I. C. Khoo, *Electrically assisted self-confinement and waveguiding in planar nematic liquid crystal cells* Appl. Phys. Lett. **77 n.1**, 7-9 (2000).

[12] A. De Luca, S. Nersisyan, and C. Umeton, *Observation of cancellation and second light-induced Frèdericksz transition in nematic liquid crystals* Opt. Lett. **28**, 108–110 (2003).

[13] N. V. Tabiryan, A. Sukhov, and B. Y. Zel'dovich, *The orientational optical nonlinearity of liquid crystals* Mol. Cryst. Liq. Cryst. **136**, 1–139 (1986).

[14] A. Yariv, *Quantum electronics- 3rd ed.* (Jhon Wiley & Sons, 1987).

[15] E. Santamato, G. Abbate, P. Maddalena, and A. Sasso, *Two beam mirrorless optical bistability in nematic liquid crystal film* Mol. Cryst. Liq. Cryst. **143**, 113–122 (1987).

[16] E. Santamato, G. Abbate, R Calselice, P. Maddalena, and A. Sasso, *All-optical-field-induced first-order frèedericksz transitions and hysteresis in a nematic film* Phys. Rev. A **37**, 1375 (1988).

[17] I.C.Khoo, *Theory of optically induced molecular reorientations and quantitative experiments on wave mixing and the self-focusing of light* Phys. Rev. A **25**, 1636–1644 (1982).

[18] F. Bloisi, L. Vicari, F. Simoni, G.Cipparrone, and C. Umeton, *Self-phase modulation in nematic liquid-crystal films: detailed measurements and theoretical calculations* J. Opt. Soc. Am. B **5**, 2462–2466 (1988).

[19] M. Warenghem, J.F. Henninot and G. Abbate, *Non linearly induced self waveguiding structure in dye doped nematic liquid crystals confined in capillaries* Opt. Express **2 n.12**, 483-490 (1998).

[20] R. Caputo, A.V. Sukhov, N.V. Tabyrian, C. Umeton and R.F. Ushakov *Mass transfer processes induced by inhomogeneous photopolymerisation in a multicomponent medium* Chemical Physics, **271 (3)** 323-335 (2001)

[21] B.Ya. Zel'dovich, S.R. Nersisyan and N.V. Tabiryan *Threshold interaction of extraordinary light waves with nemtics* Zh. Eksp. Teor. Fisz. **88** 1207-1217 (1985)

[22] D. Duca, C. Umeton and N.V. Tabiryan *Unperturbing observation of orientational states of nematics* Opt. Comm. **93** 103-106, (1992)

Chapter 2

Light propagation in periodic and non-periodic potentials

We present a simple model which enables the derivation of light propagation in a generic dielectric structure starting from Maxwell's equations. Discrete diffraction and soliton solutions for a periodic profile of the refractive index are numerically derived in a waveguide array without assumption of discrete eigenmodes or Bloch functions. For a sinusoidal periodic profile, results are in good agreement with theoretical data and experimental results already reported in literature. Furthermore, the direct derivation performed by means of a general approach allows to extend the analysis to a generic structure with no periodic conditions. As particular cases, light propagation in a double gaussian profile and in an alternated, non-periodic refractive index profile are reported.

2.1 Introduction

In the last few years, non-linear optical effects in waveguide arrays have been intensively studied, both experimentally [1–4] and theoretically [1, 3–8] by exploiting models that refer to the "Fermi-Pasta-Ulam" approach to one-dimensional dynamical systems [9]. This approach analyzes an interaction between neighbors that contains nonlinear terms. Numerical models have been implemented by exploiting the Coupled-Mode Theory (CMT) [5]: By considering only nearest-neighbor interactions, it has been shown that the optical electric field propagating in the nth waveguide obeys a nonlinear difference-differential equation; each waveguide is coupled only to the adjacent channels and can be described via a 'coupling constant', which is proportional to an overlap integral of two adjacent modes [2, 5]. In the continuum (or long-wavelength) approximation, this discrete process can be described by the non-linear Schrödinger equation [5, 10, 11]. This approach has played an important role in understanding the observed effects, providing, in particular, fundamental relations between those parameters (like array period and beam incidence angle) that enable to manage the discrete diffraction phenomenon [1, 6, 10]. In fact, by combining these relations with the diffraction equation, it is possible to predict whether the light beam experiences normal diffraction (the beam spreads while propagating), anomalous diffraction (the beam spreads while propagating, but some anomaly is observed) or if diffraction disappears [1–3, 12]. The limit of this theory is represented by the sharp discreteness that has to be hypothesized for the nonlinear periodic system, according to which the dielectric structure exists only in the waveguides with a high refractive index. Besides the CMT approach, the Floquet-Bloch (FB) analysis, which is applicable also to lossy waveguides [4, 13–15], has

been used to extend concepts introduced in the CMT, by making a preliminary analysis of the modes which can propagate in the array. In the framework of this model, it is necessary to make use of the Bloch theorem (born in the field of solid state physics), which states that eigenfunctions of the Schrödinger equation for the case of a periodic potential structure exhibit the same periodicity of the potential structure [16]; therefore, wave equation solutions result to have the same periodicity of the refractive index modulation Δn. In this way, the FB approach, while well enabling investigation of light propagation in periodic structures, prevents extending the study to those cases in which the physical system does not exhibit any periodicity. In investigating discrete diffraction, also another approach has been exploited, which is able to predict the beam evolution in non-periodic systems too: It is the (non-linear) beam propagator method (BPM), a simulation technique used to study the propagation of electromagnetic waves in inhomogeneous media [17, 18]. Availability of solutions depends on the possibility of dividing light propagation over a very small distance Δz into two actions: the first one is concerned with the divergence of the beam in a medium without index variation, while the second one is related to the modification of the phase front due to the index modulation [19]. In principle, this approach is not necessarily restricted to beams that propagate at small angles with respect to the optical axis of the system, as explicitely required, instead, by the CMT and FB theory (in whose frameworks, however, the technique can be used). Unfortunately, the BPM is valid only for small spatial variation Δn of the refractive index.

2.2 Theoretical model

We present a simple model that enables to investigate propagation of light in a medium with a modulated transverse profile of the refractive index. The novelty and interest of our approach is in showing that, under suitable conditions, discrete diffraction and discrete solitons can be obtained by simply coupling the Maxwell equations with this "index modulated" medium, without any necessity of an "a priori" discretization of the equations and any necessity of all the different kind of approximations that have to be necessarily used in all the papers cited in our references. Our model is very simple, general ed elegant, but implies that obtained equation can be solved only by using a numerical approach. The propagation of the optical field $\mathbf{E}(x, z)$ is analyzed in the xz-plane while the beam impinges on a sample whose refractive index $n(x)$ varies along the x-direction only. We analyze the problem by directly starting from Maxwell's equations, without supposing any discreteness of the medium neither a periodicity of the solutions; we want to stress, indeed, that we perform a numerical analysis of Maxwell's equations which makes use "only" of the Slowly Varying Envelope Approximation (SVEA) on the optical electric field. We hypothesizes a solution of the kind: $\mathcal{E}(\xi, \zeta, t) = \mathbf{e}(\xi, \zeta) \exp[-i(\tilde{\mathbf{k}} \cdot \tilde{\mathbf{r}} - \omega t)]$ where $\mathbf{e} = \mathbf{E}/E_0$ is the normalized electric field, E_0 being the field amplitude, ξ and ζ are the normalized coordinates $\xi = x/D$, $\zeta = z/D$, D being the sample thickness, $\tilde{\mathbf{r}} = (\xi, \zeta)$, $\tilde{\mathbf{k}} = (k_\xi, k_\zeta)$ is the normalized light propagation constant with modulus $|\tilde{\mathbf{k}}| = 2n\pi D/\lambda$, λ indicates the wavelength of the optical field and n is the refractive index of the medium where light is coming from. Under these conditions, the Maxwell's wave equation becomes:

$$\frac{\partial \mathbf{e}}{\partial \zeta} + \frac{i}{2k_\zeta}\frac{\partial^2 \mathbf{e}}{\partial \xi^2} + \frac{k_\xi}{k_\zeta}\frac{\partial \mathbf{e}}{\partial \xi} + \frac{i\tilde{k}_0^2}{2k_\zeta}\left[n^2(\xi) - n^2\right]\mathbf{e} = 0, \tag{2.1}$$

where $\tilde{k}_0 = 2\pi D/\lambda$ and $n(\xi)$ indicates the transverse profile of the refractive index. In order to solve equation 2.1 we utilize a numerical technique based on a finite-differences scheme for both spatial derivatives (with respect to ξ, ζ spatial directions). We create a lattice of computational grid points (i, j) in the ξ-ζ plane, where lattice steps $\Delta\xi$ and $\Delta\zeta$ allow to go from i to $i + 1$ and from j to $j + 1$ respectively. Evolution of the optical field in the ζ direction is then simulated by determining the value of the field at the $(i, j + 1)$ point by means of the field values at previous points. All simulations have been carried out by putting $D = 100\mu m$, $\lambda = 532nm$ and $n = 1$, while $\Delta\zeta$ and $\Delta\xi$ are chosen case by case in such a way that numerical stability of solutions is ensured.

Reliability of the model has been checked by comparing obtained numerical results with both experimental and theoretical data already reported in literature. In fact, from literature [1] it is well known that, indicating by k_x the transverse component of the impinging light wavevector and by Λ the transverse periodicity of the refractive index of the medium, by choosing discrete values of Λ ($\Lambda = [2m + 1]\lambda/2$, m integer) in the interval $\pi/2 < |k_x\Lambda| \leqq \pi$ the light beam experiences anomalous discrete diffraction. In fact, light distribution tends to broaden while propagating (like in normal diffraction) but most of the light concentrates in two distinct outermost lobes. Moreover, diffraction completely disappears around the two values $k_x = \pm\pi/2\Lambda$. We have applied our model to the case of a sinusoidal transverse modulation of the refractive index: $\Delta n = \Delta n_{max} \sin(2\pi\xi/\tilde{\Lambda})$ where $\tilde{\Lambda}$ indicates a normalized periodicity ($\tilde{\Lambda} = \Lambda/D$).

2.3 Numerical solution and Results

Results for the case $\Delta n_{max} = 0.04$ and $\tilde{\Lambda} = 0.02926$ ($m = 5$) are reported in Fig. 2.2 and 2.1 where the beam intensity is represented in the (ξ, ζ) plane. It is

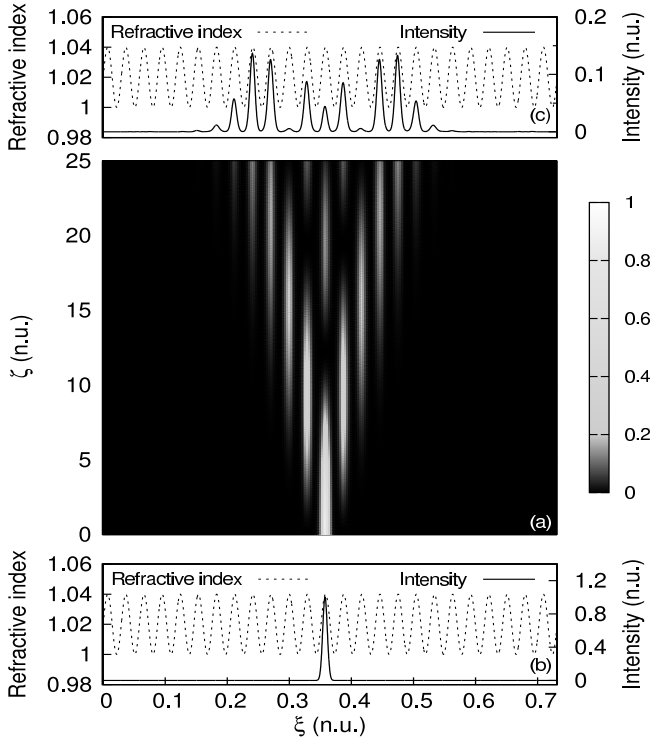

Figure 2.1: *(a) Top view of the normal discrete diffraction of light in a waveguide array; (b) and (c) are the refractive index and the intensity profile at the cell input and output respectively. All values are reported in normalized units (n.u.). Also intensity is normalized to 1.*

well evident that, if only one waveguide is excited, most of the light is concentrated into two distinct outermost lobes, reproducing the solution obtained with CMT in the discrete diffraction problem (Green's function) [3, 4]. The simulation well reproduces results reported in [3, 4] but, besides these results, our model predicts also normal discrete diffraction and discrete soliton: An initially localized excita-

tion (more than one waveguide is excited simultaneously), tends to spread over the whole array, as in continuous systems (Fig. 2.2 and Fig. 2.1) [3].

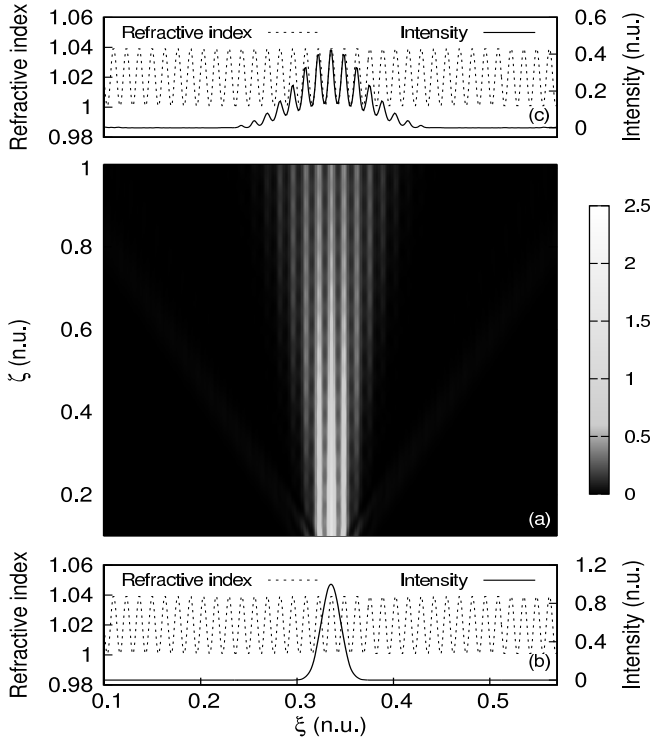

Figure 2.2: *(a) Top view of the anomalous discrete diffraction of light in a waveguide array; (b) and (c) are the refractive index and the intensity profile at the cell input and output respectively. All values are reported in normalized units (n.u.). Also intensity is normalized to 1.*

Appearance of discrete diffraction also depends on the propagation direction and on the incidence angle [3]; in particular cases, diffraction can be completely suppressed and a discrete soliton appears, which moves across the array. As shown in Fig. 2.3, also this particular case, numerically solved by using our approach, confirms the validity of the model which proves suitable to predict all kind of results available in literature.

Our approach becomes irreplaceable when we try to understand what happens

if the physical system does not exhibit any periodicity and variations of the refractive index values are not small. Let us consider, first, the particular case in which

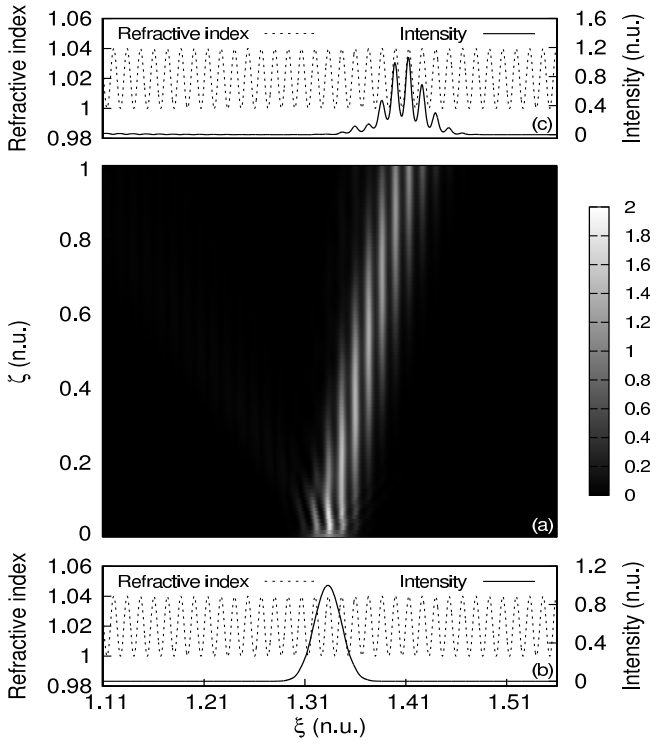

Figure 2.3: *(a) Top view of the propagation of light in a sinusoidal lattice for the case of a non zero incidence angle; (b) and (c) represent the refractive index and the intensity profile at the cell input and output respectively.*

the waveguide array is formed only by two waveguides, which exhibit a gaussian transverse profile of the refractive index. We consider the behavior of a focused gaussian beam injected in a single guide (right guide of Fig. 2.4): upon propagation, the optical power is periodically exchanged between the two guides; this result is also reported in [3, 20], where, however, the approach can take into account only the values of the refractive index in the waveguides, without allowing to manage a more realistic transverse modulation of this material parameter. The theoretical

"switch-like" behavior simulated by our model is confirmed by plotting, along the ζ direction, the intensity profile in the central part of every guide (inset of Fig.2.4).

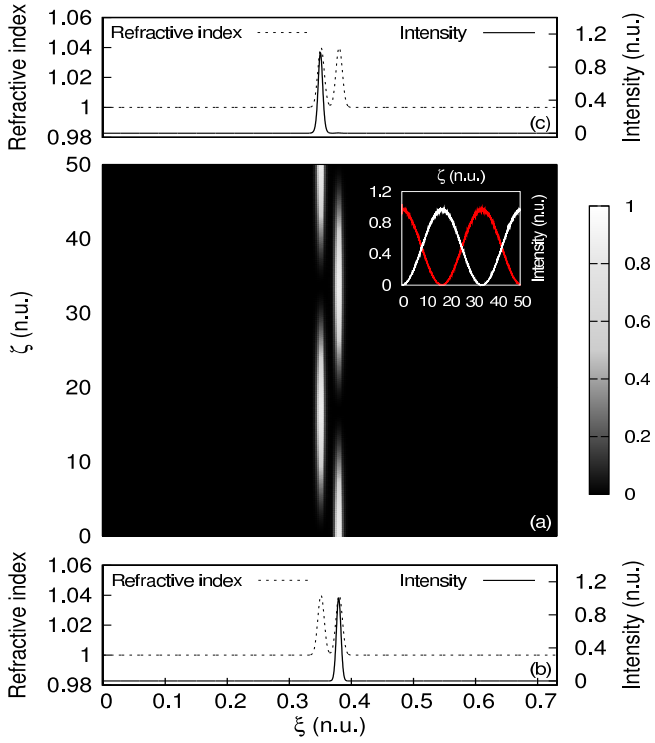

Figure 2.4: *(a) Top view of the "switch-like" behavior of light in a non-periodic structure made of two waveguides with a gaussian refractive index profile. (b) and (c) are the refractive index and the gaussian intensity profile at the cell input and output respectively. The inset represent the intensity profile along the ζ direction, in the central part of every guide.*

Obtained functional curves behave like $\cos^2(\zeta)$ and $\sin^2(\zeta)$ and a total energy transfer between the two waveguides is observed.

Very interesting is also the case of the field evolution of a gaussian beam in an alternated, but non-periodic structure. In particular, we have designed a refractive index profile in which the spacing between the different gaussian waveguides linearly increases by starting from the center of the sample. We have obtained the

formation of anomalous discrete diffraction until this space becomes so large that there is no coupling between transverse modes; the optical field is reflected by the structure and a sort of multi-guide "discrete beats" behavior starts, as shown in Fig. 2.5.

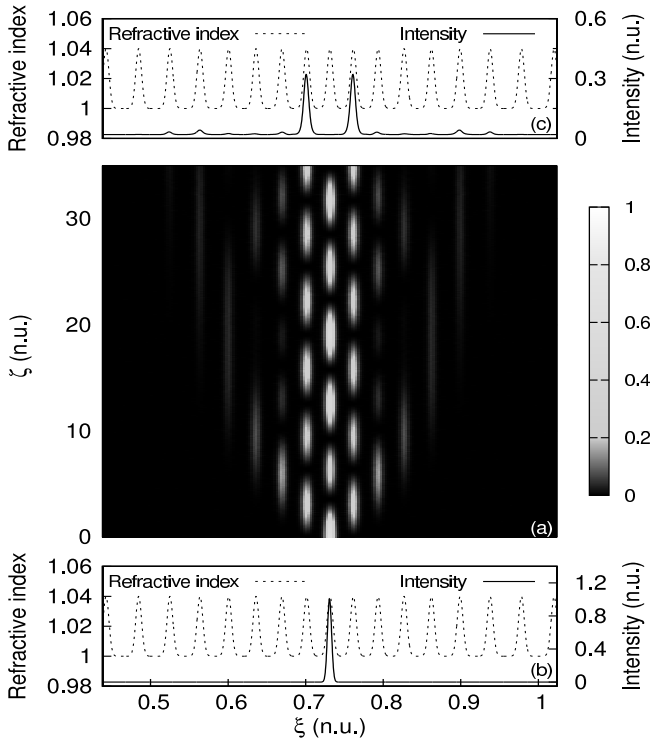

Figure 2.5: *(a) Top view of the "discrete beats" behavior of light in a non-periodic structure made of waveguides spaced by a distance that linearly increases by starting from the center of the sample; (b) and (c) are the refractive index and the gaussian intensity profile at the cell input and output respectively.*

We stress that, at our knowledge, only our model is able to reproduce this case in which no periodicity is imposed and Δn can reach values as high as 0.56, a case that is not reported in this letter, but has been used in one of our numerical simulations.

2.4 Conclusions

In conclusion we have presented a simple model which, starting directly from Maxwell's equations, is able to predict all the kind of known discrete phenomena, like normal, anomalous discrete diffraction and discrete solitons, related to light propagation in an optical wavegide array. The approach exhibit several advantages in comparison with models used up to now: It is directly derived from Maxwell's equations written in the medium of interest, with the only limitation of the "Slowly Varying Envelope Approximations"; it is not necessary to introduce any "coupling constant" which determines the transverse propagation of the optical field "canceling" the existence of a different medium between two waveguides (CMT model); it is not limited to small modulations of the transverse profile of the refractive index (BPM approach). Finally it is not necessary to hypothesize any periodicity in the transverse profile of the refractive index of the medium (FB model) and, in fact our approach enables to predict also the propagation of light in non-periodic systems. Two examples have been reported: the first one is related to the "switch-like" behavior obtained in a structure made of two adjacent waveguides, each of them exhibiting a gaussian transverse profile of the refractive index; the second one is related to an alternated, but non-periodic system in which the structure is made of (gaussian) waveguides spaced by a distance that linearly increases by starting from the center of the sample. In both cases, new and interesting light propagation behaviors have been predicted.

Bibliography

[1] H. S. Eisenberg, Y. Silberberg, R. Morandotti, and J. S. Aitchison. *Phys. Rev. Lett.*, 85:1863–1866, (2000).

[2] R. Morandotti, H. S. Eisenberg, Y. Silberberg, M. Sorel, and J. S. Aitchison. *Phys. Rev. Lett.*, 86(15):3296–3299, (2001).

[3] F. Lederer and Y. Silberberg. *Optics and Photonics News*, pages 49–53, (2002).

[4] D. N. Christodoulides, F. Lederer, and Y. Silberberg. lattices. *Nature*, 424:817–823, (2003).

[5] D. N. Christodoulides and R. I. Joseph. *Opt. Lett.*, 13:794–796, (1988).

[6] M. J. Ablowitz and Z. H. Musslimani. *Phys. Rev. E*, 65:056618, (2002).

[7] J. M. Bendickson, J. P. Dowling, and M. Scalora. *Phys. Rev. E*, 53:4107–4121, (1996).

[8] Falk Lederer, Sergey Darmanyan, and Andrey Kobyakov. *Spatial Solitons*. Springer-Verlag Berlin Heidelberg New York, 2001. pag. 269-292.

[9] E. Fermi, Pasta J, S. Ulam, and M. Tsingou. *(Los Alamos Scientific Laboratory of the University of California) Tech. Rep.*, LA-1940 (Report written May 1955). Los alamos scientific laboratory of the university of california.

[10] Amnon Yariv. *Optical Electronics*. Saunders College Publishing, 1991.

[11] S. Suntsov, K. G. Makris, D. N. Christodoulides, and G.I. Stegeman. *Phys. Rev. Lett.*, 96:063901, 2006.

[12] G. I. Stegeman and M. Segev. diversity. *Science*, 286:1518–1522, 1999.

[13] D. Mandelik, H. S. Eisenberg, Y. Silberberg, R. Morandotti, and J. S. Aitchison. floquet-bloch solitons. *Physical Review Letters*, 90:053602, 2003.

[14] Nai-Hsiang Sun, J. K. Butler, G. A. Evans, L. Pang, and P. Congdon. floquet-bloch theory. *Journal of Lightwave technology*, 15:2301–2315, 1997.

[15] A. Fratalocchi, G. Assanto, K.A. Brzdakiewicz, and M.A. Karpierz. *Optics Express*, 13:1808–1815, 2005.

[16] Charles Kittel. *Introduction to solid state physics*. New York, 1996.

[17] M. D. Feit and J. A. Fleck. *Applied Optics*, 17:3990–3997, 1978.

[18] Lars Thylèn and Chung Ming Lee. *J. Opt. Soc. Am.A*, 9:142–146, 1992.

[19] M. Shalaby. *Pure Applied Optics*, 5:9971004, 1996.

[20] Tullio Rozzi and Andrea Di Donato. *Componenti e circuiti ottici*. Tecnoprint S.n.c., 2005.

Chapter 3

Director configuration in a NLC cell with multiple interfaces

The study of optical solitons and light filaments steering in liquid crystal requires the utilization of particular cells designed for top view investigation and realized with an input interface which enables to control the molecular director configuration and to prevent light scattering. Actually, the director orientation imposed by this additional interface is estimated only by experimental observations. We report a simple model describing the distribution of the director orientation inside a liquid crystal sample under the anchoring action of multiple interfaces. The model is based on the elastic continuum theory and strong anchoring is taken into account for boundary conditions. Results are in good agreement with experimental observations.

3.1 Introduction

In order to investigate the interaction between light waves and liquid crystalline materials, the latter are confined into cells made of glass plates or quartz slabs, separated by Mylar spacers or silicon balls. The obtained liquid crystal (LC) film is usually acted on by a focused laser beam that impinges normally to the plates, in this way, the maximum film thickness that can be involved in the interaction with light is about 100 μm. In the last years, optical phenomena that occur over propagation distances of some millimiters have required a different design of LC cells. The waveguide regime imposed, for example, by solitary wave propagation [1–5] led to utilize suitable cell configurations, all adopting a further glass slab for the input of the light beam [1–8] (Fig. 3.1). The interface of this slab, suitably treated by the same anchoring processes used for top and bottom surfaces, represents both a way to prevent light scattering and a mean to control the director configuration from the input to the bulk, the supposed director distribution being based, however, on estimations deduced from experimental observations. Simulation of director orientation in different configurations has been reported in numerous articles during the last decades also in case of general elastic coefficient [9], hybrid alignment [10] and also cylindrically [11] and spherically [12, 13] confined nematic. Anyway these models were developed in order to solve problems of major importance in liquid crystal displays, optical fibers and polymer dispersed liquid crystal confinements and appear to be less useful when discussing interface effects in liquid crystal cells realized for the study of optical solitons. In this paper we present a detailed theoretical study of the director configuration in samples with particular boundary conditions. This is fundamental to understand why optical phenomena like the contemporary forma-

tion of both extraordinary and ordinary waves (or the propagation of light filaments), have been observed only in some particular cell configurations [5–8].

3.2 Experiments

In Fig. 3.1 we present our system, that is a NLC cell with glass plates behaving as optical interfaces at the input as well as at the output of the cell. The main role

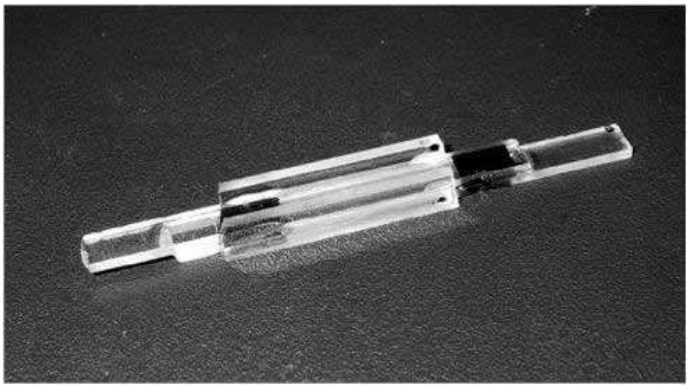

Figure 3.1: *Image of the cell realized with input and output interfaces*

of these interfaces is to prevent a possible random director orientation due to the presence of a meniscus at the cell input (thus fixing the exact value of refractive index in that point). Furthermore, it has been recently found that new interesting phenomena can be observed controlling the interface anchoring [14]. In Fig. 3.2 we report different effects observed in light filaments which are achievable only in particular cell configurations. The cases taken into account refer to three configurations of the nematic director inside the cell, realized by using different surface anchoring conditions. We indicate these configurations by $[\sigma_\alpha/\sigma_\beta]$, where σ_α represents the angle between the x-axis and the anchoring direction at the input interface, while σ_β represents the angle between the z-axis (propagation direction) and the anchor-

ing direction of both upper and lower interfaces. In particular, we have considered $[0°/0°]$ or standard configuration, $[0°/45°]$ and $[45°/45°]$ In the case of standard

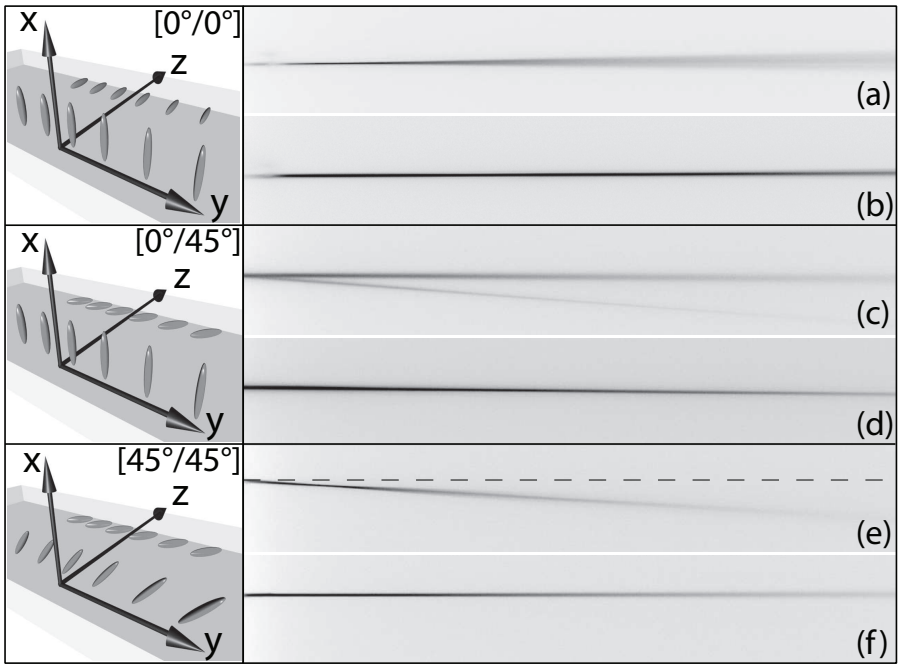

Figure 3.2: *Sketches on the left represent the three particular cell configuration:* $[0°/0°]$, $[0°/45°]$ *and* $[45°/45°]$. *Inverted grayscale images on the right are acquired from the top of the relative liquid crystal cell: (a) and (b) represent the linear diffraction and nematicon formation, in the case of standard configuration* $[0°/0°]$, *respectively. The formation of the e- and o-waves is presented in (c) while (d) shows the soliton formation by starting from these two waves in the case of* $[0°/45°]$ *cell configuration. In (e) and (f) the e-wave only is created by using the* $[45°/45°]$ *cell configuration. The steering of this light filament over angles larger than* $7°$ *is obtained by applying an external AC voltage.*

configuration $[0°/0°]$ we obtain linear diffraction without application of an external electric field, and optical spatial soliton (nematicons [1]) formation by applying an external quasi-static electric field (Figs.3.2(a) and 3.2(b)). The formation of the *e* and *o*-waves in the case of $[0°/45°]$ cell configuration is reported in Fig. 3.2(c), while Fig. 3.2(d) shows the nematicon formation by starting from these two waves.

In Fig. 3.2(e) the *e*-wave only is created by using the $[45°/45°]$ cell configuration; the steering of this light filament over angles larger than $7°$ is obtained by applying an external AC voltage (Fig. 3.2(f)).

3.3 Three interfaces model

We analyze the steady state solutions of our system, starting from Frank's equations [15, 16] and imposing three boundary conditions at the glass interfaces. In details, the sample is represented in the sketch of Fig. 3.3(b), where α is the input interface, while β_1 and β_2 are the top and bottom ones. The molecular director ($\vec{n}$) configuration is described by angles θ and φ represented in figure 3.3(a).

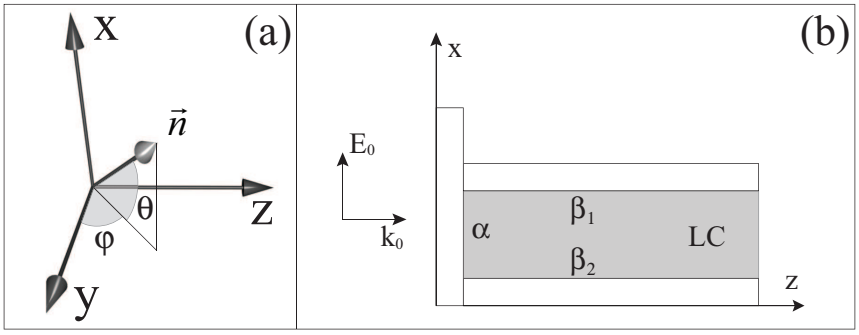

Figure 3.3: *(a) 3D sketch of the axes orientation and θ and φ angles used to describe the orientation of the director $\vec{n}$ in the sample. (b) Side view of a LC cell with an input interface used to prevent random director orientation. α, β_1 and β_2 are the three anchoring interfaces.*

Being D the cell thickness, it is useful to introduce normalized coordinates $\xi = x/D$ and $\zeta = z/D$. The steady state Frank's elastic equations for θ and φ reduce

therfore to:

$$\frac{\partial^2\theta}{\partial\xi^2}+\frac{\partial^2\theta}{\partial\zeta^2}+\sin\theta\cos\theta\left[\left(\frac{\partial\varphi}{\partial\xi}\right)^2+\left(\frac{\partial\varphi}{\partial\zeta}\right)^2\right]=0 \tag{3.1}$$

$$\cos^2\theta\left(\frac{\partial^2\varphi}{\partial\xi^2}+\frac{\partial^2\varphi}{\partial\zeta^2}\right)\sin 2\theta\left(\frac{\partial\theta}{\partial\xi}\frac{\partial\varphi}{\partial\xi}+\frac{\partial\theta}{\partial\zeta}\frac{\partial\varphi}{\partial\zeta}\right)=0. \tag{3.2}$$

Equations (3.1) and (3.2) are coupled, highly non linear and do not admit analytical solutions; therefore, in order to avoid further approximations, we have used a numerical approach. We have introduced on the right hand the time dependent terms: $\partial\theta/\partial\tau$ in eq. 3.1 and $\partial\varphi/\partial\tau$ in eq. 3.2, where $\tau = t/\tau_R$ is a normalized time and τ_R is the tipical relaxation time for LC: $\tau_R = \gamma D^2/\mathcal{K}$ (where γ is the viscosity and $\mathcal{K}$ the elastic constant in the one constant approximation $\mathcal{K}_1 = \mathcal{K}_2 = \mathcal{K}_3 \equiv \mathcal{K}$). Starting from the configuration needed to match the boundary conditions, we let the system evolve until the steady state is reached. We have used a second order Runge-Kutta scheme for temporal derivatives with a step $\Delta\tau = 10^{-5}$ normalized units (n.u.), which matches the need for stability of solutions with a reasonable computational time. For spatial derivatives, a central derivative scheme is used, where $\Delta\xi = 6\cdot 10^{-2}$ n.u. and $\Delta\zeta = 5\cdot 10^{-3}$ n.u. ensure stability of solutions.

3.4 Results

Solutions have been carried out for three different boundary conditions, corresponding to the configuration of our three particular cells used to investigate light propagation in LC [14]. In all cases taken into account, interfaces have been treated with a rubbing process that imposes a planar alignment of the LC director, with a pretilt angle of about 4°, while the distinguishing feature of the different configurations is the rubbing direction on the anchoring interfaces. The first case refers to the

3D sketch of figure 3.4 and represents the simplest and more typical configuration:

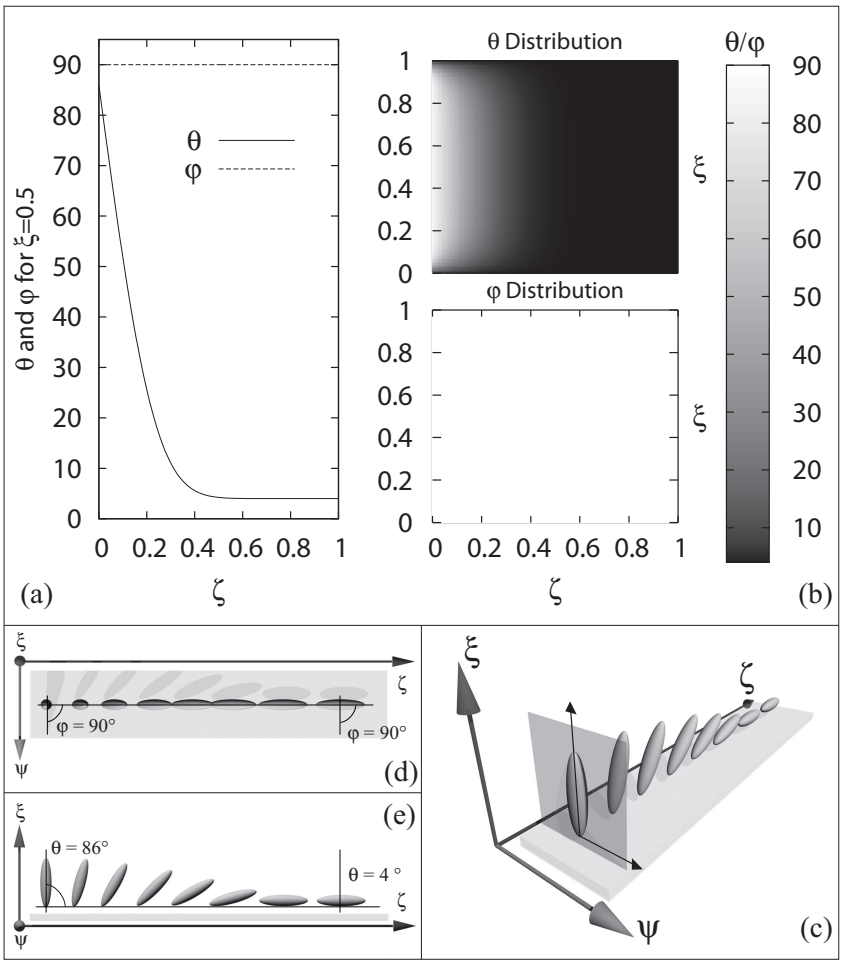

Figure 3.4: *Standard configuration [$0°/0°$]: a) Numerical solution for θ and φ behaviour at $\xi = 0.5$, presented as a function of ζ; b) Grayscale maps of θ and φ configuration in the cell c) 3D sketch representing the molecular director distribution in the center of the cell ($\xi = 0.5$); d) Top view of the 3D sketch; e) Side view of the 3D sketch.*

in this case the rubbing direction is along the x axis at the α-interface and along the z axis at the $\beta_{1,2}$-interfaces. This case is also indicated as *standard* or [$0°/0°$] configuration [14]. According to figure 3.3 and taking into account the pretilt angle, this configuration corresponds to the boundary conditions: $\varphi(\xi, 0) = 90°$, $\theta(\xi, 0) = 86°$,

$\theta(0,\zeta) = 4°$, $\varphi(0,\zeta) = 90°$, $\theta(1,\zeta) = 4°$, $\varphi(1,\zeta) = 90°$. Simulations have been carried out for a time interval necessary for the system to reach the steady state condition ($\partial\theta/\partial\tau \leq 10^{-10}$). In Fig. 3.4a the behavior of θ and φ in the center of the cell is presented as a function of ζ, while Fig. 3.4b shows bidimensional maps of θ and φ in the whole sample. It is evident that the φ-distribution remains constant

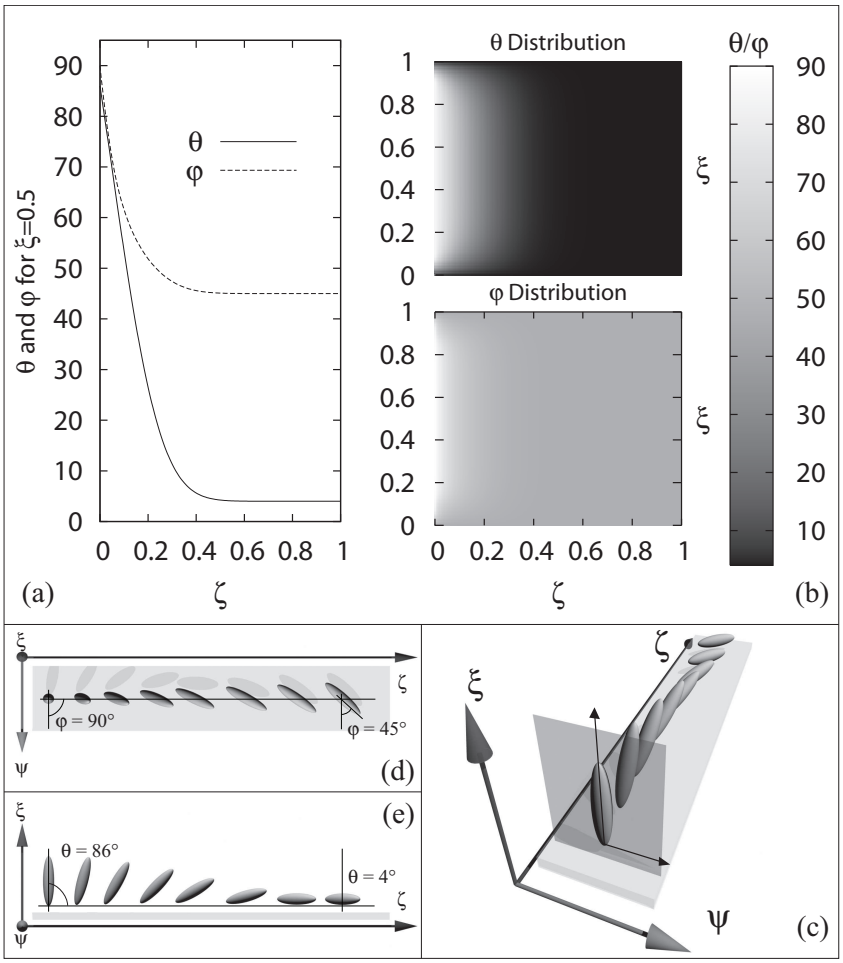

Figure 3.5: *[$0°/45°$] configuration: a) Numerical solution for θ and φ behaviour at $\xi = 0.5$ presented as a function of ζ; b) Grayscale maps of θ and φ configuration in the cell; c) 3D sketch representing the molecular director distribution in the center of the cell ($\xi = 0.5$); d) Top view of the 3D sketch; e) Side view of the 3D sketch.*

in the whole sample and the effect of the anchoring at the input interface propa-

gates into the bulk for about 0.5 normalized unit, in accordance with the predicted theoretical coherence length [15, 16]. This result is also in good agreement with the behavior estimated from experimental observations [14]. The second case of interest refers to the 3D sketch of figure 3.5 and represents a more complex configuration, referred to as $[0°/45°]$: in this case the rubbing direction is along the x direction on α but it forms an angle of $45°$ with the z-direction on $\beta_{1,2}$. In our formalism, tacking into account the pretilt angle, this configuration corresponds to the boundary conditions: $\theta(\xi, 0) = 86°$, $\varphi(\xi, 0) = 90°$, $\theta(0, \zeta) = 4°$, $\varphi(0, \zeta) = 45°$, $\theta(1, \zeta) = 4°$, $\varphi(1, \zeta) = 45°$. Also in this case, simulations have been carried out until the temporal steady state is reached. Results are shown in Fig. 3.5(a), where the behavior of θ and φ in the center of the sample is presented as a function of the normalized coordinate ζ, and in Fig. 3.5(b), where the bidimensional maps of θ and φ in the whole sample are reported. Also in this case, the predicted coherence length is about 0.5 n.u. and the φ distribution seems to be modulated in order to match the imposed boundary conditions. Results are again in good agreement with the behavior estimated from experimental observations [14].

The last considered case refers to the 3D sketch of Fig. 3.6 and represents the particular cell configuration referred to as $[45°/45°]$: in this case, the rubbing direction forms an angle of $45°$ with the x direction on α and an angle of $45°$ with the z-direction on $\beta_{1,2}$. The peculiarity of this cell is that it allows the formation of nematicons propagating inside, without any need of acting on the impinging light polarization [6,14]. This configuration corresponds, in our formalism, to the boundary conditions: $\theta(\xi, 0) = 45°$, $\varphi(\xi, 0) = 4°$, $\theta(0, \zeta) = 4°$, $\varphi(0, \zeta) = 45°$, $\theta(1, \zeta) = 4°$, $\varphi(1, \zeta) = 45°$. Also in this case, simulations have been carried out until the temporal steady state condition has been reached. Fig. 3.6(a) shows the behavior of θ and

φ in the center of the sample as a function of ζ. Fig. 3.6(b) represents the bidimensional maps of θ and φ in the whole sample. The coherence length is about 0.5 n.u., and both φ and θ distributions seems to be modulated in order to match the imposed border conditions. This result represents a further good agreement with estimations carried out from experimental observations [14].

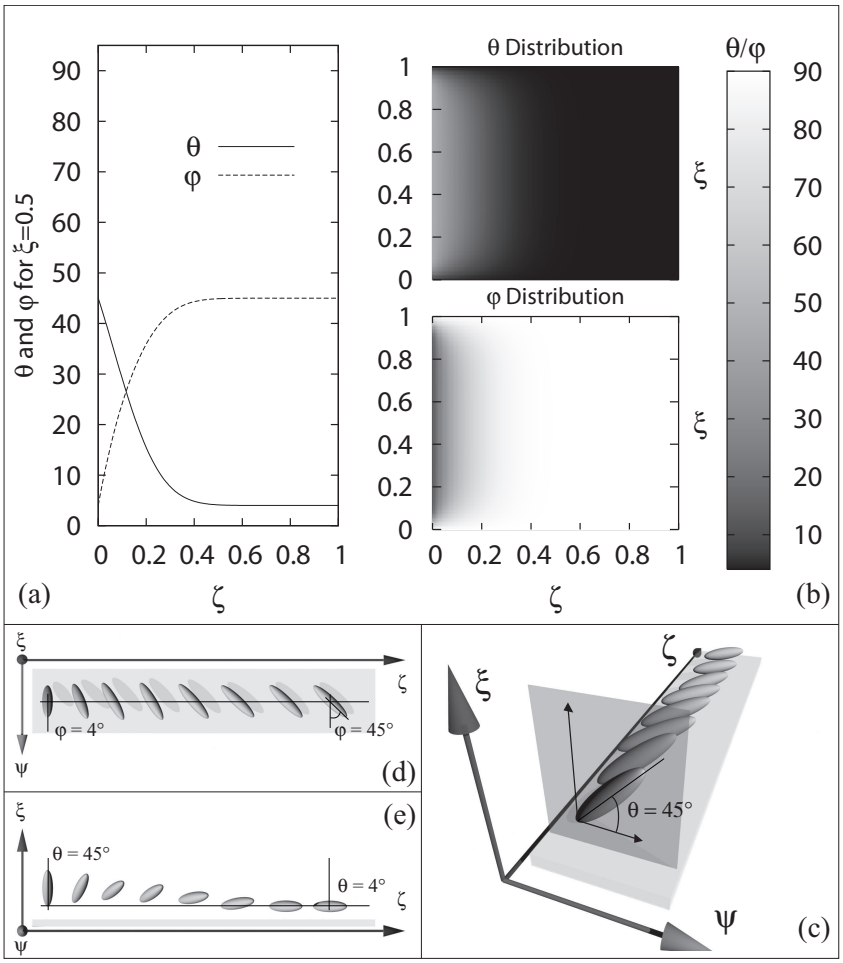

Figure 3.6: *[$45°/45°$] configuration: a) Numerical solution for θ and φ behaviour at $\xi = 0.5$ presented as a function of ζ; b) Grayscale maps of θ and φ configuration in the cell; c) 3D sketch representing the molecular director distribution in the center of the cell ($\xi = 0.5$); d) Top view of the 3D sketch; e) Side view of the 3D sketch.*

3.5 Conclusions

In conclusion, we have implemented a numerical model to characterize the input interface effects in NLC cells utilized to study optical spatial soliton (nematicon) propagation. We have investigated three particular configurations, experimentally used to observe the behavior of linearly polarized, focused, light beams propagating through the cell. These solutions are in good agreement with experimental observations. Furthermore, our model gives a reference for design, fabrication and characterization of particular liquid crystal cells that are needed to study formation and propagation of nematicons. Furthermore, this model, coupled to codes able to describe light propagation in anisotropic media (under development), will allow to advance in understanding light phenomena attributed to *interface effects*.

Acknowledgments

We acknowledge the parallel computing prompts of Francesco Principe and the support of Prof. Gaetano Assanto.

Bibliography

[1] M. Peccianti, G. Assanto, A. De Luca, C. Umeton, I.C. Khoo, Appl. Phys. Lett. **77**(1), 7 (2000)

[2] M. Peccianti, C. Conti, G. Assanto, A. De Luca, C. Umeton, Appl. Phys. Lett. **81**(18), 3335 (2002)

[3] J. Beeckman, K. Neyts, M. Haelterman, Journal of Optics A: Pure and Applied Optics **8**, 214 (2006)

[4] M. Peccianti, C. Conti, G. Assanto, A. De Luca, C.P. Umeton, Journal of Nonlinear Optical Physics and Materials **12**, 525 (2003)

[5] M. Peccianti, C. Conti, G. Assanto, A. De Luca, C. Umeton, Nature **432**, 733 (2004)

[6] A. Alberucci, M. Peccianti, G. Assanto, G. Coschignano, A. De Luca, C. Umeton, Optics Letters **30**(11), 1381 (2005)

[7] C. Conti, M. Peccianti, G. Assanto, Phys. Rev. Lett. **92**, 113902 (2004)

[8] M. Peccianti, A.K. Brzdakiewicz, G. Assanto, Optics Letters **27**(16), 3 (2002)

[9] E. Schröder, Physical Review E **62**(6), 8830 (2000)

[10] D. Krzyzanski, G. Derfel, Physical Review E **63**, 021702 (2001)

[11] R. m. Marroum, G.S. Iannacchione, D. Finotello, M.A. Lee, Physcal Review E **51**, R2743 (1995)

[12] J.H. Erdmann, S. Ẑumer, J.W. Doane, Phys. Rev. Lett. **64**, 1907 (1990)

[13] O.O. Prishchepa, A.V. Shabanov, V.Y. Zyryanov, Physical Review E **72**, 031712 (2005)

[14] A. De Luca, G. Coschignano, M. Morabito, C.P. Umeton, Optics Express **14**(12), 5548 (2006)

[15] N.V. Tabiryan, A. Sukhov, B.Y. Zel'dovich, Molecular Crystals and Liquid Crystals **136**, 1 (1986)

[16] I.C. Khoo, *Liquid Crystals: Physical Properties and Nonlinear Optical Phenomena* (Jhon Wiley & Sons, Inc., New York, 1995)

Conclusions

In conclusion, my work has been oriented to the analysis of three different topics:

- In the first one, I realized both a theoretical and an experimental work, numerical solutions of a general model for the interaction of N gaussian light beams with a physical system which is a NLC cell with strong anchoring conditions has been carried out. The model has been experimentally checked for the case of two beams in an opposite incidence angle geometry obtaining a good agreement with theoretical predictions. Local response was extensively analyzed and, under particular experimental conditions, it has been also shown that nonlocality plays an important role. Results give a new light on these kind of nonlinear media, stimulating the investigation of phenomena that can take place.

- In the second one, by realizing the theoretical analisys and numerical simulation code, I have presented a simple model able to predict all kinds of known discrete phenomena. Normal, anomalous discrete diffraction and discrete solitons, related to light propagation in an optical waveguide array was analyzed in detail. The approach exhibits several advantages in comparison with models used up to now: It is directly derived from Maxwell's equations

written in the medium of interest, with the only limitation of "Slowly Varying Envelope Approximations" (SVEA). In fact, this approach does not require the introduction of any "coupling constant" which determines the transverse propagation of the optical field "erasing" the existence of a different medium between two waveguides (CMT model); it is also not limited to small modulations of the transverse profile of the refractive index (BPM approach). Finally it is not necessary to assume any periodicity in the transverse profile of the refractive index of the medium (FB model) so, it was possible to dimonstrate that our approach enables to predict how light propagates in non-periodic systems. To enlight this feature, two examples have been reported: one related to the "switch-like" behavior obtained in a structure made of two adjacent waveguides, each of them exhibiting a gaussian transverse profile of the refractive index; the other related to an alternated, non-periodic system in which the structure is made of (gaussian) waveguides spaced by a distance that linearly increases by starting from the center of the sample. Both cases, have shown new and interesting light propagation behaviors have been predicted. Design of experiments devoted to check our approach in detail is under development.

- In the third one, a numerical model whas been implemented to characterize the input interface effects in NLC cells utilized to study optical spatial soliton propagation. Three particular configurations, experimentally utilized to observe the behavior of light beams propagating through the cell, has been theoretical investigated providing solutions in good agreement with experimental observations. Our model gives also a reference for design, fabrication

and characterization of liquid crystal cells usefull for studing formation and propagation of nematicons. Furthermore, this model, coupled to codes able to describe light propagation in anisotropic media (under development), will allow contribute to the understanding of light phenomena attributed to *interface effects*.

In conclusion, during my doctorate in the LICRYL laboratory of ' *ottica veloce*' in the University of Calabria I realized both experimental and numerical work. In particular, during the three years of Ph.D I have reenphatized my theoretical skills. For this purpose I attended a school in CINECA (Bologna, Italy) for learning parallel computing. In the framework of HPC-Europe program (High Performance computing), I also visited the high performance computing center HLRS in Stuttgart (Germany) and the IWM Fraunhofer institute for Mechanics of Materials in Freiburg (Germany). In that occasion I improved my skills by learning new parallel thecniques and realized my code for light propagation in a cell with multiple interfaces.

Publications

1. Veltri A. , **Pezzi L.** , De Luca A. , Umeton C. P.

   "Different reorientational regimes in a liquid crystalline medium undergoing multiple irradiation"

   Optics Express, 2007, Vol. 15, n. 4, pp. 1663-1671

2. **Pezzi L.** , Veltri A. , De Luca A. , Umeton C. P.

   "Model for molecular director configuration in a liquid crystal cell with multiple interfaces"

   JNOPM (2007) Vol. 16, No. 2 Pages 199-206

3. **Pezzi L.**; A. Veltri; A. De Luca; C. Umeton

   "Non-Linear Effects in NLC Media Undergoing Two Beams Irradiation"

   MCLC Molecular Crystals and Liquid Crystals; April 2007; Volume 465 No. 1 Pages 71 - 80

4. De Luca A. , Veltri A. , **Pezzi L.** , Coschignano G. , Umeton C. P. , Alberucci A. , Conti C. , Peccianti M. , Assanto G.

   "Nematic Liquid Crystal Cells for Optical spatial solitons (Nematicons)"

   SPIE The international Society for Optical Engineering 2007 Vol. 6487, pp. 64870R-1 - 64870R-8.

Ringraziamenti

Il primo rigraziamento lo voglio rivolgere al mio collega Alessandro, un amico e un collega che auguro a tutti di avere, senza il quale il mio lavoro di dottorato sarebbe stato molto più difficile. Devo a lui le mie basi di informarica dalle quali ho costruito il mio lavoro di dottorato e buona parte di quello che sono riuscita ad imparare a livello professionale e umano in questo ambiente universitario. Il resto lo devo ad Antonio un collaboratore preciso e puntuale che ha avuto molta pazienza con me, la cui assenza in questo momento si sente parecchio. Insieme a loro sono riuscita a costrire lavori dalla doppia matrice teorico-sperimentale che hanno esaltato e completato le mie capacità.

A seguire vorrei ringraziare Luciano, Melissa e Roberto membri del laboratorio di ottica 'più veloce del west' uno dei pochi laboratori dove la competizione fra i membri non trascende in tensioni che renderebbero l'ambiente meno vivibile.

Per ultimo, come si addice al capo (come negli articoli), il prof. Umeton, che ha sempre svolto alla perfezione il suo ruolo di capo supervisore.

Ci sono poi le mie due amiche e colleghe Sameh e Marialuigia senza le quali sarebbe stato tutto molto più triste.

Non posso poi dimenticare gli amici e quasi colleghi Luca Guzzardi e Francesco Principe il cui piccolo apporto al mio lavoro è stato comunque importante per migliorarne la qualità.

Ed infine, ma non perchè ultimi, la mia famiglia: mia madre, mio padre e mio fratello, parte della mia vita da sempre, che credono in me più di quanto io creda in me stessa, che hanno sempre saputo come sostenermi e dirmi i si e i no giusti; e mio marito Andrea il mio sostegno e il mio futuro, a cui dedico il lavoro di questi tre anni, lo dedico al suo spirito di sopportazione e alla sua capacità di compredermi.